UNIVERSIDADE FEDERAL DE UBERLÂNDIA
Programa de Pós - Graduação - INFIS
Gustavo Diniz Silva

Reentrant Kondo effect in a quantum impurity coupled to a metal-semiconductor hybrid contact

Brasil

2020

UNIVERSIDADE FEDERAL DE UBERLÂNDIA
Programa de Pós - Graduação - INFIS
Gustavo Diniz Silva

Reentrant Kondo effect in a quantum impurity coupled to a metal-semiconductor hybrid contact

Dissertação apresentada ao Programa de Pós-graduação em Física da Universidade Federal de Uberlândia, como requisito parcial para obtenção do título de mestre em Física Teórica. Área de Concentração: Física da Matéria Condensada.

Universidade Federal de Uberândia – UFU

Insituto de Física - INFIS

Programa de Pós-Graduação

Orientador: Prof. Dr. George Balster Martins

Coorientador: Prof. Dr. Edson Vernek

Brasil

2020

Dados Internacionais de Catalogação na Publicação (CIP)
Sistema de Bibliotecas da UFU, MG, Brasil.

S586r 2020

Silva, Gustavo Diniz, 1995-
Reentrant Kondo effect in a quantum impurity coupled to a metal-semiconductor hybrid contact [recurso eletrônico] / Gustavo Diniz Silva. - 2020.

Orientador: George Balster Martins.
Coorientador: Edson Vernek.
Dissertação (mestrado) - Universidade Federal de Uberlândia, Programa de Pós-Graduação em Física.
Modo de acesso: Internet.
Disponível em: http://doi.org/10.14393/ufu.di.2020.3609
Inclui bibliografia.
Inclui ilustrações.

1. Física. I. Martins, George Balster, 1962-, (Orient.). II. Vernek, Edson, 1973-, (Coorient.). III. Universidade Federal de Uberlândia. Programa de Pós-Graduação em Física. IV. Título.

CDU: 53

Nelson Marcos Ferreira - CRB-6/3074

UNIVERSIDADE FEDERAL DE UBERLÂNDIA
Coordenação do Programa de Pós-Graduação em Física
Av. João Naves de Ávila, 2121, Bloco 1A, Sala 213 - Bairro Santa Mônica, Uberlândia-MG, CEP 38400-902
Telefone: (34) 3239-4309 - www.infis.ufu.br - cpgfisica@ufu.br

ATA DE DEFESA - PÓS-GRADUAÇÃO

Programa de Pós-Graduação em:	Física				
Defesa de:	Dissertação de Mestrado				
Data:	Vinte de fevereiro de 2020	Hora de início:	10:15	Hora de encerramento:	12:20
Matrícula do Discente:	11812FIS004				
Nome do Discente:	Gustavo Diniz Silva				
Título do Trabalho:	*Reentrant Kondo effect in a quantum impurity coupled to a metal-semiconductor hybrid contact*				
Área de concentração:	Física				
Linha de pesquisa:	Sistemas fortemente correlacionados				
Projeto de Pesquisa de vinculação:	Many-body physics in Majorana and Weyl fermion systems				

Reuniu-se na Sala de Vídeo Conferência da PROPP, Bloco 3P, Campus Santa Mônica, da Universidade Federal de Uberlândia, a Banca Examinadora, designada pelo Colegiado do Programa de Pós-graduação em Física, assim composta: Professores Doutores: Gerson Ferreira Júnior - INFIS/UFU; Diogo de Oliveira Soares Pinto - USP/SC e George Balster Martins INFIS/UFU orientador(a) do(a) candidato(a).

Iniciando os trabalhos o(a) presidente da mesa, Dr(a). George Balster Martins, apresentou a Comissão Examinadora e o candidato(a), agradeceu a presença do público, e concedeu ao Discente a palavra para a exposição do seu trabalho. A duração da apresentação do Discente e o tempo de arguição e resposta foram conforme as normas do Programa.

A seguir o senhor(a) presidente concedeu a palavra, pela ordem sucessivamente, aos(às) examinadores(as), que passaram a arguir o(a) candidato(a). Ultimada a arguição, que se desenvolveu dentro dos termos regimentais, a Banca, em sessão secreta, atribuiu o resultado final, considerando o(a) candidato(a):

Aprovado.

Esta defesa faz parte dos requisitos necessários à obtenção do título de Mestre.

O competente diploma será expedido após cumprimento dos demais requisitos, conforme as normas do Programa, a legislação pertinente e a regulamentação interna da UFU.

Nada mais havendo a tratar foram encerrados os trabalhos. Foi lavrada a presente ata que após lida e achada conforme foi assinada pela Banca Examinadora.

Documento assinado eletronicamente por **Diogo de Oliveira Soares Pinto**, **Usuário Externo**, em 20/02/2020, às 16:58, conforme horário oficial de Brasília, com fundamento no art. 6º, § 1º, do Decreto nº 8.539, de 8 de outubro de 2015.

Documento assinado eletronicamente por **George Balster Martins**, **Presidente**, em 20/02/2020, às

17:10, conforme horário oficial de Brasília, com fundamento no art. 6º, § 1º, do Decreto nº 8.539, de 8 de outubro de 2015.

Documento assinado eletronicamente por **Gerson Ferreira Junior**, **Professor(a) do Magistério Superior**, em 21/02/2020, às 10:28, conforme horário oficial de Brasília, com fundamento no art. 6º, § 1º, do Decreto nº 8.539, de 8 de outubro de 2015.

A autenticidade deste documento pode ser conferida no site https://www.sei.ufu.br/sei/controlador_externo.php?acao=documento_conferir&id_orgao_acesso_externo=0, informando o código verificador **1885145** e o código CRC **C1069DE8**.

Referência: Processo nº 23117.012529/2020-16 SEI nº 1885145

Agradecimentos

Primeiramente a minha mãe Girlene Firmina Diniz, e a minha Irmã Yngrid Martins Diniz, as pessoas mais importantes na minha vida. Quero agradecer também ao meu Tio Leomar José da Silva, pelo seu papel de pai durante minha criação.

Aos meus avós Augusta Maria Godinho e Sebastião Martins Godinho, por todo o carinho durante todos esses anos.

Ao meu orientador Dr. Edson Vernek pela possibilidade de realizar este projeto, além de toda a orientação e auxílio oferecidos no decorrer do trabalho.

Ao prof. Dr. George Balster Martins por assumir minha orientação no final do trabalho e por todo o auxílio fornecido.

Ao prof. Dr. Ginetom Souza Diniz pelos resultados encontrados para o AGNR, o que enriqueceu muito o nosso trabalho.

Aos meus amigos (não vou citar nomes, pois são muitos) e colegas do INFIS. E também à todos os amigos dentro e fora da Universidade Federal de Uberlândia.

À Universidade Federal de Uberlândia e ao Instituto de Física pela oportunidade de realizar esse curso.

Por fim, a CAPES pelo apoio financeiro.

Abstract

In this work, we study the physics of a magnetic impurity coupled to several conduction band structures (metallic band, pseudo-gap systems and semiconductors with finite gap). However, the main focus is to explain the behavior of a system comprising a quantum impurity, strongly coupled to a semiconductor (with gap 2Δ) and weakly coupled to a metal. Using the Numerical Renormalization Group (NRG) and Anderson's poor man's scaling, we show that this system (Impurity+metal-semiconductor hybrid contact), displays a *reentrant* Kondo stage as one gradually lowers the temperature. The analysis of the corresponding Single Impurity Anderson Model (SIAM), through the impurity's thermodynamic and spectral properties, shows that the *reentrant* stage is characterized by a second sequence of SIAM fixed points, viz., free orbital (FO) $\rightarrow$ local moment (LM) $\rightarrow$ strong coupling (SC). In the higher temperature stage, the SC fixed point (with a Kondo temperature T_{K1}) is unstable, while in the lower temperature, the Kondo screening exhibits a much lower Kondo temperature T_{K2}, associated to a stable SC fixed point. The results clearly suggest that the *reentrant* Kondo screening is associated to an effective SIAM, with an effective Hubbard U_{eff}, whose value is clearly identifiable in the impurity's local density of states. This *reentrant* SIAM, or effective SIAM, at temperatures below the gap, behaves as a *replica* of the high temperature SIAM. We show this in our results, and more specifically, in the NRG flow diagram (obtained through NRG). The second stage RG flow, whose FO fixed point emerges for $T \approx \Delta < T_{K1}$, takes over once the RG flows away from the unstable first stage SC fixed point. The intuitive picture that emerges from our analysis is that the first Kondo state develops through impurity screening by semiconducting electrons, while the second stage involves screening by metallic electrons, once the semiconducting electrons are out of reach to thermal excitations ($T < \Delta$) and only the metallic (low) spectral weight inside the gap is available for impurity screening. For all parameter ranges analyzed, we find through the NRG results that $T_{K2} \ll T_{K1}$. Last, we analyze a hybrid system formed by a quantum impurity 'sandwiched' between an armchair graphene nanoribbon (AGNR) and a scanning tunneling microscope (STM). In this system, the energy gap (2Δ) can be externally tuned by an electric-field-induced Rashba spin-orbit interaction. We analyzed this system for realistic parameter values, using NRG, and concluded that the *reentrant* SIAM, and the second stage Kondo, is worthy of experimental investigation.

Keywords: Kondo Temperature, Critical Coupling, *reentrant* Kondo, *reentrant* SIAM, Armchair graphene nanoribbon

Resumo

Nesse trabalho, estudandos a física de uma impureza magnética acoplada a várias bandas de condução (banda metálica, pseud-gap e semicondutora). Porém, o foco principal do trabalho é explicar o comportamento de um sistema constituido por uma impureza quântica, fortemente acoplada a um semicondutor (com gap 2Δ) e fracamente acoplada a um contato metálico. Usando Rernoamlização de Grupo Numérica (NRG) e *poor man's scaling* no Modelo de Anderson, mostramos que para esse sistema (impureza+metal+semicondutor), exibe um estágio *repetição* do efeito Kondo à medida que diminui gradualmente a temperatura. A análise do correspondente Modelo de Anderson de uma única impureza (SIAM), através das propriedades termodinâmicas e espectrais da impureza, mostra que o estágio de *repetição* é caracterizado por uma segunda sequência de pontos fixos SIAM, Orbital Livre (FO) $\rightarrow$ Momento Local (LM) $\rightarrow$ acoplamento forte (SC). No estágio de temperatura mais alta, o ponto fixo SC (com uma temperatura Kondo T_{K1}) é instável, enquanto o segundo Kondo tem uma temperatura Kondo T_{K2} muito mais baixa, associada a um ponto fixo SC estável . Os resultados sugerem claramente que a repetição está associada a um SIAM efetivo, com um pico de Hubbard U_{eff}, cujo valor é claramente identificável na densidade de estados local da impureza.Esse SIAM efetivo para baixa temperatura, que chamamos de *repetição* do SIAM, se comporta como uma *réplica* do SIAM de alta temperatura. O fluxo RG do segundo estágio (obtido através do NRG), cujo ponto fixo FO emerge por $T \approx \Delta < T_{K1}$, assume o controle assim que o RG flui para longe do ponto fixo SC instável do primeiro estágio. A imagem intuitiva que emerge de nossa análise é que o primeiro estado de Kondo se desenvolve por meio da blindagem da impureza por elétrons semicondutores, enquanto o segundo estágio envolve a blindagem por elétrons metálicos, uma vez que os elétrons semicondutores estão fora do alcance das excitações térmicas ($T < \Delta$) e apenas os elétrons metálicos, dentro do gap estão disponíveis para a blindagem da impureza. Para todos os intervalos de parâmetros analisados, através do NRG encontramos $T_{K2} \ll T_{K1}$. Por último, nós analizamos um sistema hibrido formado por uma impureza 'imprensada' entre uma nanofita de grafeno armchair (AGNR) e um microscópio de tunelamento de varredura (STM). Nesse sistema, a energia do gap (2Δ) pode ser externamente alterada por um campo elétrinco induzido por interação spin-orbita Rashba. Analizamos esse sistema para parâmetros realísticos, usando NRG, e concluimos que a *repetição* do SIAM, e o segundo estágio Kondo, pode ser investigado experimentalmente.

Palavras Chaves: Temperatura Kondo, Acoplamento Crítico, *repetição* do Kondo, *repetição* do SIAM, Nanofita de grafeno armchair

List of Figures

Contents

1 Introduction

Unraveling the physics of a many-body interacting system is always a challenging task. Despite simplicity form of mutual interactions between pairs of its constituents, collectively, the system ofttimes behaves in an unexpected manner. This fascinating facet of nature has been beautifully discussed in a seminal paper by P. W. Anderson [3]. The archetypal example, in condensed matter physics, is that of the ground state of the many-body Kondo problem [4, 5, 6]. Experimentally observed in the thirties, the Kondo effect remained incognito until the sixties, when the Japanese physicist J. Kondo explained the phenomena [4]. The phenomena consist of a collective dynamical screening of a localized magnetic moments embedded in a conducting material. The antiferromagnetic coupling between the localized magnetic moments and the spins of the itinerant electrons renders a singlet-like many-body ground state in the system. The characteristic energy associated to this phenomena is related to the so called Kondo temperature T_K, below which the screening takes place. Originally, observed in bulk material doped with iron [7, 8], later on the Kondo effect have been investigated in a variety of different systems such as magnetic atoms on metallic surfaces and quantum dot (QD) coupled to conduction electrons [9, 10, 11, 12].

The comprehension of the physical mechanisms underlying the Kondo screening was important to understand magnetic properties in many materials. In nanoscopic systems, the Kondo effect plays a pivotal role in transport properties, which is relevant to electronic devices [13, 14, 15, 16, 17]. For example, in single electron transistors [18], when the Kondo effect takes place, the system exhibits an resonant many-body electronic level that is responsible for the electronic transport across the device. This dramatic effect in the transport properties nanoscopic systems has profound implications in technological applications [19]. More recently, renewed interest in the Kondo effect has been noted in the context of topological materials such as topological insulators [20, 21, 22, 23, 24, 25].

To explain the Kondo effect, J. Kondo proposed a Hamiltonian describing the main spin-flip scattering processes involved in the phenomena. Later on, it was shown that the Kondo Hamiltonian could be derived from the more general Anderson model in the regime in which charge fluctuations are suppressed [26]. It is unfortunate, however, that it is not possible to solve the Anderson model in an exact manner. The reason is that the coulomb interaction term together with the infinite degrees of freedom of the conduction electrons in the Hamiltonian result in a rich and complicated many-body problem, to which there is no known exact solution.

Nevertheless, the Anderson model can be investigated using different techniques and approximations, such as Green's functions method [27], a slave bosons in mean-field approximation [28], non-crossing approximation [29], perturbation theory [30], etc. As we mention above, one interesting strategy to address the Kondo effect is to derive the Kondo Hamiltonian from the Anderson model. Even though this approach simplifies the problem, the resulting Kondo Hamiltonian is not yet exactly solvable. The advantage, however, is that within the Kondo model we can employ more easily the scaling analysis, a technique that allows us to obtain some relevant physical quantities of the problem, such as the Kondo temperature [31]. In some particular case it is also instructive to apply scaling analysis in Andereson Model [32]. Despite the usefulness of the many approximation solutions for the Anderson and Kondo models, they fail to properly describe the ground state of the system. To properly address the Kondo problem, Wilson developed a very powerful numerical renormalization group (NRG) method capable to properly tackle the Kondo problem [6, 26, 5].

A renormalization-group analysis of the single impurity Anderson Model (SIAM) [6, 26, 5] shows that the system crosses over three different fixed points as the temperature is lowered: (i) the unstable free orbital (FO) fixed point, in which the impurity is effectively decoupled from the conduction band, (ii) the local moment (LM) fixed point (also unstable), where the impurity acquires a highly fluctuating magnetic moment, and (iii) the stable strong coupling (SC) fixed point, in which the magnetic moment of the impurity becomes fully screened by the electrons of the conduction band. The SIAM, so to speak, provides a rich, although the simplest, description of the Kondo physics in QDs. The scenario presented above represents a generic picture of the physics of the SIAM, which remains qualitatively valid, provided the density of states of the conduction electrons exhibits no special features close to the Fermi level. Richer Kondo physics can be found if the conduction band exhibits structures such as a pseudo-gap or zero-energy peaks, like van-Hove singularities. These features have been studied in great detail by several authors [33, 34, 35, 36].

It is known that the Kondo effect is strongly dependent on the character of the conduction band to which the magnetic impurity is coupled [33]. A richer Kondo physics emerge when the conduction band exhibits some structures near the Fermi level. For instance, in pseudo-gap systems, in which the conduction band density $\rho(\varepsilon)$ of states depends on the energy ε as ε^r, with $0 < r < 2$, there is a critical Kondo coupling below which there is no screening [37]. Also working with pseudo-gap system, Cheng *et al.* [32] found the SIAM fixed points using poor man's scaling in Anderson Model.

An interesting, but less studied situation, is the case in which the conduction band is that of a semiconductor, i.e, a spectra characterized by a finite gap Δ. Beyond conventional narrow-gap semiconductors, examples of such a gapped material encompass trans-Polyacetylene [38], also Dirac insulators [39] and the armchair graphene nanoribbon

(AGNR) [40, 41, 42, 43, 44]. The richness of the Kondo physics resulting from the interplay between T_K and Δ has been studied since almost three decades ago using a variety of numerical and analytical techniques. For instance: Quantum Monte Carlo (QMC), by Takegahara *et al.* [45, 46] and T. Saso [47], poor man's scaling, $1/N$ expansion, non-crossing approximation (NCA) and QMC, by Ogura and Saso [48], equation-of-motion plus Hartree-Fock, by Cruz *et al.* [49], density matrix renormalization group (DMRG), by Yu and Guerrero [50], numerical renormalization group (NRG), by Takegahara *et al.* [45, 46] and Chen and Jayaprakash [51], Density Matrix NRG (DM-NRG), by Moca and Roman [52], as well as perturbation theory and the local moment approach, by Galpin and Logan [53, 54].

The earliest results pointed to the existence of a Kondo ground state (a SC fixed point) whenever $\Delta < \Delta_c$, where the critical gap Δ_c should fulfill the relation $\Delta_c \lesssim T_K$, being T_K defined as the Kondo temperature for $\Delta = 0$. However, NRG results [45, 51, 52] have indicated that a finite critical gap Δ_c only exists *away* from half-filling, while at half-filling any arbitrarily small gap (i.e., any $\Delta > 0$) results in the ground state becoming a doublet, i.e., switching from the standard Kondo-singlet SC fixed point (for $\Delta = 0$) to a doublet LM fixed point. This qualitative difference (half-filling vs. away-from-half-filling) has been confirmed by analytical calculations [53] and a local-moment approach [54], where it was shown that the ground state away from half-filling is a so-called generalized Fermi liquid, while it is a non-Fermi liquid for all finite values of Δ at half-filling. In addition, DM-NRG calculations [52] studied the quantum phase transition (QPT) occurring away from half-filling for $\Delta = \Delta_c$ and showed the formation of a single bound state when the system is in the SC regime ($\Delta < \Delta_c$), and the formation of an additional one once the system transitions to the LM regime ($\Delta > \Delta_c$).

In this work we, investigate the Kondo effect in a physical system that is a slightly different model from the one already analyzed in the studies described above, as it is composed of a QD [or a quantum impurity (QI)] that is *s*trongly coupled, on the right, to a semiconducting lead (with a gap 2Δ) and, on the left, *w*eakly coupled to a *metallic* lead (see Fig. 1). We aim at comparing the results from the poor man's scaling analysis to the NRG approach obtained for the system as it is composed of a QD that is *s*trongly coupled, on the right, to a semiconducting lead and, on the left, is *w*eakly coupled to a *metallic* lead. More specifically, we want to compare two quantities: the Kondo temperature T_K and the critical Kondo couplings J_c, obtained from the semiconductor conduction bands with gap by the two approaches. In addition, we want to explain the unusual behavior of this system for energy scales below the gap and propose a real system where this can be observed.

The main result of this work is obtained by poor man's scaling (PMS) and NRG analysis, of the appropriate SIAM for modeling the first system mentioned in the preceding

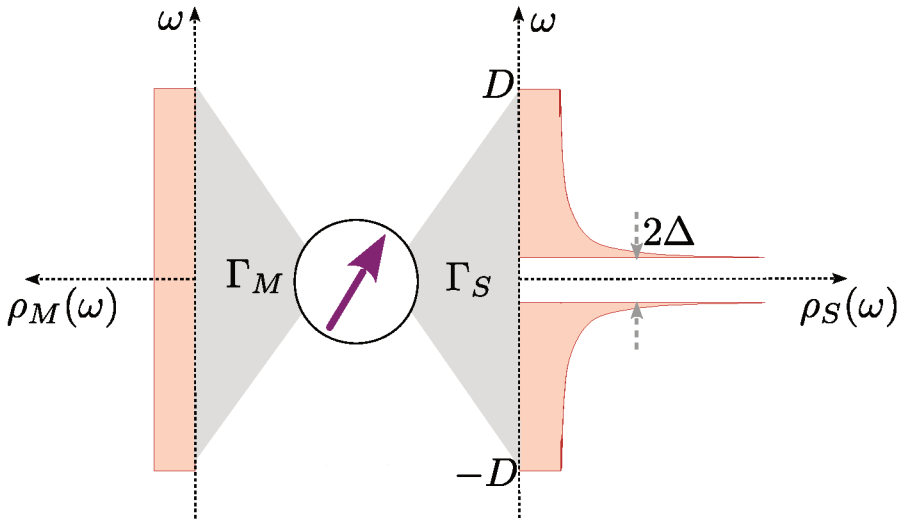

Figure 1 – Schematic representation of a QD coupled to a metallic lead (left) and to a semiconducting lead (right). The metallic lead is represented by a flat density of states $\rho_M(\omega)$, while the semiconducting lead is modeled by an energy dependent density of states $\rho_S(\omega)$ characterized by a gap 2Δ. D is a cutoff energy and represents the bandwidth of conduction electrons and is taken as our energy unit.

paragraph, reveals, as one lowers the temperature, a sequence of two Kondo *stages*. Both are characterized by sequences of SIAM fixed points (FO-LM-SC), where the higher temperature SC fixed point, characterized by a Kondo temperature T_{K1}, is unstable, while the second stage has a stable SC fixed point and has a much lower Kondo temperature T_{K2}. We dub the lower-temperature Kondo-state as a '*reentrant* Kondo state', which is associated to an 'emergent' effective SIAM, with an effective Hubbard U_{eff}, in contrast to the 'bare' SIAM associated to the first stage Kondo effect. Our findings have been theoretically investigated in a realistic system composed by a quantum impurity coupled to an armchair graphene nanoribon and to an STM tip suggest that the reentrant Kondo state can be experimentally observed.

This dissertation is organized as follows: In chapter 2 we discuss the appropriate models for the magnetic impurity coupled to a conduction band like the Anderson model and the Kondo model. In chapter 3, using the PMS, we find the scale equations for each of the models mentioned. In chapter 4 we defined the model for the impurity coupled to more than one lead, in addition we find the scaling equations for our system composed of an impurity coupled to a semiconductor-lead and weakly coupled to a metallic-lead. In chapter 5 we show the NRG calculations for our system and for AGRN system, and in In chapter 6 we conclude this work.

2 Models for magnetic impurities coupled to structured conduction bands

The Kondo effect results from unusual scattering mechanisms of conduction electrons in a metal due to magnetic impurities. These scattering processes renders a term in the electrical resistivity that increases logarithmically with temperature as the temperature T is lowered. These mechanisms can also be used, more generally, to describe many-body scattering processes from impurities or ions having quantum mechanical degrees of freedom compatible with those of the conduction electrons. In this more general sense, these mechanisms have become a key concept in condensed matter physics in understanding the behavior of metallic systems with strongly interacting electrons.

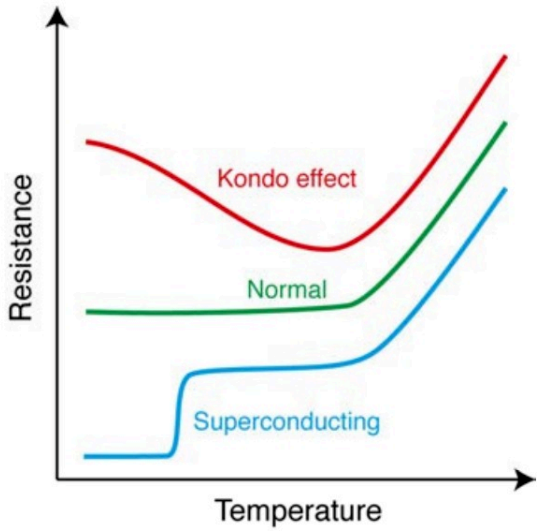

Figure 2 – (red) Schematic representation of the resistance curve observed when the conduction electrons are blinded by the magnetic impurity. This behavior can be observed in systems that have magnetic impurities. In these systems it is possible to observe a resistance minimum as the temperature decreases and this is the first experimental evidence of the Kondo effect. (green) Schematic representation of the resistance curve observed for 'normal' metals and explained by the phonon scattering mechanism. (blue) Schematic representation of the resistance for superconductors metals where the resistance drops to zero below a critical temperature, this phenomenon is explained by the mechanisms of Cooper pairs. Figure retired from [1].

For conventional conductors, the resistance should decrease gradually, since the temperature decreases, scattering due to phonons are suppressed [55]. In superconductors, on the other hand, as the temperature decreases, there is an emergent stable ground state, called superconducting state, in which all the conduction electrons form the so called Cooper pairs [56]. In the case of Kondo problem in turn, a third scenario, different from the previous ones, is observed. At high temperatures the electrons in the conduction band have enough energy to ignore the presence of magnetic impurities. However, as the temperature drops, the electrons in the conduction band start “feeling" the magnetic moment of the impurities in the material, coupling antiferromagnetically to it. As the temperature further decreases, these electrons form a cloud around the impurity forming, coectively, the so called Kondo singlet state. Electrons far from the Kondo cloud are more efficiently scattered, resulting in the enhancement of the resistance. This rather complex situation is explained correctly through the spin scattering mechanism.

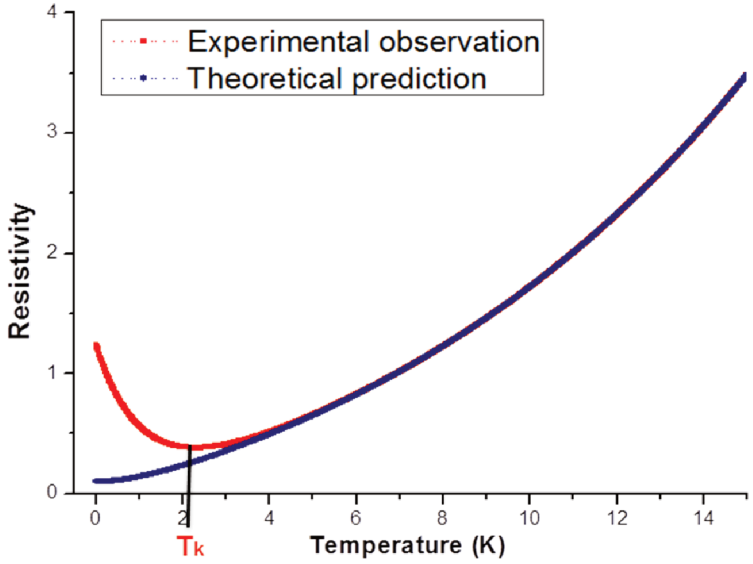

Figure 3 – Schematic of the resistivity graph for metal with Kondo Effect. The divergences between the predictions are significant at low temperatures, close to the characteristic temperature T_K where the resistivity minimum is observed. Figure adapted from W. J. de Haas and G. J. van den Berg, Physica vol. 3, page 440, 1936.

To better understand the Figs. 2 and 3, here we will discuss briefly the resistivity,without going into the details of the calculations. The resistivity as function of the temperature T, in the low-temperature regime, can be written as the contribution due to Fermi liquid properties, phonon scatterings plus the contribution due the scattering by magnetic impurities in metal. In the first two mechanisms leads to terms depending on the temperature as T^2 and T^5 [55]. However, as explained by Kondo, the contribution to restivity by the spin-flip mechanism is logarithmic [4]. So the total contribution to the

resistivity is given by

$$R(T) \approx R_0 \left[1 + \alpha T^2 + \beta T^5 - \gamma \ln\left(\frac{k_B T}{D - \varepsilon_F}\right)\right], \tag{2.1}$$

where α, β and γ are parameters that depend on the material. For small temperatures, the logarithmic term in equation above increase as the temperature decreases, explaining the resistivity minimum observed in the Fig. 3.

2.1 Anderson and Kondo Model

To understand the behavior of a magnetic impurity coupled to the conduction band and also the scattering mechanisms responsible for the Kondo effect, we start with the single impurity Anderson model (SIAM) described in second quantization as

$$H_A = \sum_\sigma \varepsilon_d d_\sigma^\dagger d_\sigma + U n_{d\uparrow} n_{d\downarrow} + \sum_{\mathbf{k}\sigma} \varepsilon_{\mathbf{k}\sigma} c_{\mathbf{k}\sigma}^\dagger c_{\mathbf{k}\sigma} + \sum_{\mathbf{k}\sigma} \left(V_{\mathbf{k}\sigma} d_\sigma^\dagger c_{\mathbf{k}\sigma} + \text{H.c.}\right). \tag{2.2}$$

Here, $d_\sigma^\dagger$ creates (annihilates) an electron with energy ε_d and spin σ in the quantum impurity and $c_{\mathbf{k}\sigma}^\dagger$ creates and electron with energy $\varepsilon_{\mathbf{k}}$ and spin σ in the conduction band. In the above, $n_{d\sigma} = d_\sigma^\dagger d_\sigma$ is the number operator. The conduction band is characterized by a density of states $\rho(\omega) = \rho_0 f(\omega)\Theta(D - |\omega|)$ in which D is the band width, ρ_0 is a normalization factor and $f(\omega)$ is a general function that describe the shape of the density of states. For example, in the flat band $f(\omega) = 1$ or in a pseudo-gap systems $f(\omega) = \omega^r$ and in semiconductor $f(\omega) = \frac{|\omega|}{\sqrt{\omega^2 - \Delta^2}}\Theta(|\omega| - \Delta)$.

The Kondo regime manifests itself at low temperatures and when the impurity has a localized magnetic moment. In the Anderson model, the impurity is represented by a quantum dot and only has the resulting localized magnetic moment if the impurity have one unpaired electron, this is true only in the single level case. Thus, to recover this regime through the Anderson model, we will use the general Hamiltonian projection in the single occupancy subspace using the projection operators.

As already mentioned, in the Anderson model the magnetic impurity can assume three states of occupation. The empty state, where there are no electrons in the impurity, the single occupation where there is only one electron (with spin up or down) and the double occupation, the impurity has two electrons (one up and one down due to principle of Pauli's exclusion).

A comparison of the energies associated to these occupations of the impurity is represented by Figure 4. The energy of the single occupancy level is represented by E_1, while the energy difference between the double and single occupation state is $\varepsilon_d + U$, where U is the Coulomb repulsion. Thus, if the energy of the singly occupied state is much lower that the energy of the empty and doubly occupied state, then the impurity will prefer to

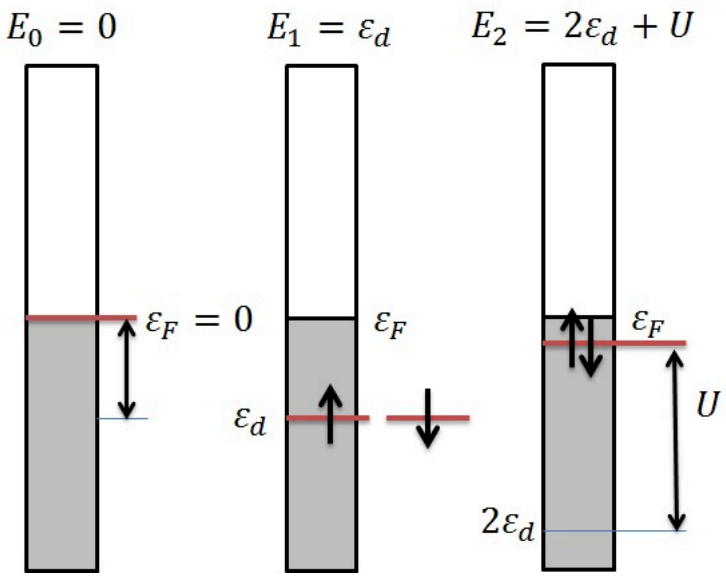

Figure 4 – Schematic representation of the impurity states and their energy. In the empty state $|0\rangle$, where there are no electrons in the quantum impurity is represented by $E_0 = 0$ in energy scale. The single occupation $|1_\sigma\rangle$ have one electron with spin σ (up or down), this state is represented by E_1 in energy scale and is extremely important in the Kondo physics since in this setting the quantum impurity has a resulting magnetic moment. Other case is the quantum impurity with two electrons, the double occupation state $|2\rangle$ with energy E_2. The double occupation have one electron spin up and one spin down by Pauli exclusion principle.

be in a single occupation state in low-energy, a necessary condition for the Kondo effect to take place.

For the impurity in a single occupied state and at low temperatures, we can use the Kondo Hamiltonian described by

$$H_{\mathrm{K}} = \sum_{\mathbf{k}\sigma} \varepsilon_{\mathbf{k}\sigma} c^\dagger_{\mathbf{k}\sigma} c_{\mathbf{k}\sigma} + \sum_{\mathbf{k}\mathbf{k}'} J_{\mathbf{k}\mathbf{k}'} \left[S^z \left(c^\dagger_{\mathbf{k}\uparrow} c_{\mathbf{k}'\uparrow} - c^\dagger_{\mathbf{k}\downarrow} c_{\mathbf{k}'\downarrow} \right) + S^+ c^\dagger_{\mathbf{k}\downarrow} c_{\mathbf{k}'\uparrow} + S^- c^\dagger_{\mathbf{k}\uparrow} c_{\mathbf{k}'\downarrow} \right]. \quad (2.3)$$

Here, $J_{\mathbf{k},\mathbf{k}'}$ is called Kondo-like coupling. A Hamiltonian like (2.3) was proposed by Kondo in 1963 [4], It was latter shown that it can be derived by performing a Schrieffer-Wolf transformation [5] to the Hamiltonian (2.2). However there is another way to do this transformation, a simpler one, using the approximation where the impurity is in a single occupation. To do this, as already commented, we will project the Anderson Hamiltonian in the single occupancy subspace to find the effective Kondo Hamiltonian.

2.2 Relation between Anderson and Kondo models

To show the connection between the Kondo and Anderson Hamiltonian in a little more detail, let us write the Anderson model in the occupation representation [see Hamiltonian in (2.4)]. In this representation, we will use the basis (in bracket notation) $|0\rangle$ for empty state, $|1_\sigma\rangle$ for single occupation with spin σ, and $|2\rangle$ for double occupation.

The resulting Hamiltonian on this basis reads

$$H_{\text{occ}} = \begin{bmatrix} H_{00} & H_{01} & H_{02} \\ H_{10} & H_{11} & H_{12} \\ H_{20} & H_{21} & H_{22} \end{bmatrix}, \tag{2.4}$$

where the matrix elements H_{ij} are found by projection operators P_i,

$$H_{ij} = P_i H_A P_j. \tag{2.5}$$

The term H_{ij} in the Hamiltonian connects the occupation subspace $|i\rangle$ and the occupation subspace $|j\rangle$. In another notation, the impurity state can be represented by the number of electrons up and down so that the state $|n_{d,\uparrow}, n_{d,\downarrow}\rangle$ where $n_{d,\uparrow}$ is the number of electrons up and $n_{d,\downarrow}$ the number of electrons down.

To find the matrix elements we need to define the projection operators for each sub-space as

$$\begin{aligned} P_0 &= (1 - n_{d\uparrow})(1 - n_{d\downarrow}), \\ P_1 &= n_{d\uparrow} + n_{d\downarrow} - 2n_{d\uparrow}n_{d\downarrow}, \\ P_2 &= n_{d\uparrow}n_{d\downarrow}. \end{aligned} \tag{2.6}$$

Note that if one apply the operator P_i in the state $|n_{d,\uparrow}, n_{d,\downarrow}\rangle$ the results will be $\delta_{n_{d,\uparrow}+n_{d,\downarrow},i}$, this can be easily confirmed by operating the operators in the possible states.

The matrix elements in Hamiltonian (2.4) can be found by equation (2.5) using the projection operators (2.6) in the Anderson model. After applying the projector and some manipulations, we find matrix elements

$$\begin{aligned} H_{00} &= \sum_{\mathbf{k},\sigma} \varepsilon_{\mathbf{k},\sigma} n_{\mathbf{k},\sigma}, \\ H_{01} &= \sum_{\mathbf{k},\sigma} V_{\mathbf{k}}^* (1 - n_{d,\bar{\sigma}}) c_{\mathbf{k},\sigma}^\dagger d_\sigma, \\ H_{02} &= 0, \\ H_{11} &= \sum_{\sigma} \left(\varepsilon_d + \sum_{\mathbf{k}} \varepsilon_{\mathbf{k},\sigma} n_{\mathbf{k},\sigma} \right) (1 - n_{d,\bar{\sigma}}) n_{d,\sigma}, \\ H_{12} &= \sum_{\mathbf{k},\sigma} V_{\mathbf{k}}^* n_{d,\bar{\sigma}} c_{\mathbf{k},\sigma}^\dagger d_\sigma, \\ H_{22} &= \left(2\varepsilon_d + U + \sum_{\mathbf{k}} \varepsilon_{\mathbf{k},\sigma} n_{\mathbf{k},\sigma} \right) n_{d,\bar{\sigma}} n_{d,\sigma}. \end{aligned} \tag{2.7}$$

As expected, these Hamiltonians are Hermitian $H_{ji} = H_{ij}^*$. In the Anderson Hamiltonian (2.4), the magnetic impurity can not migrate from empty state to the double occupation directly, then the matrix elements H_{02} and H_{20} are zero. The elements H_{00}, H_{11} and H_{22} represents, respectively, the Hamiltonian with eigenvalue of energy E_0 for the empty state, E_1 for the single occupation and E_2 for the double occupation. In addition,

the expected value of the term H_{00} ($\langle H_{00}\rangle = E_0$) at temperature $T = 0$ is exactly the energy of the Fermi level $\varepsilon_F = 0$.

Now that the Hamiltonian elements have been found, we can use the time-independent Schrödinger equation $\mathbf{\Psi} H_{\text{occ}} = E\mathbf{\Psi}$ (where $\mathbf{\Psi} = [\psi_0, \psi_1, \psi_2]^T$ in matrix form and E is the energy of the quantum impurity) to isolate the contribution of the Hamiltonian in the sub-space of single occupation ($\psi_1 H_{\text{eff}} = E\psi_1$),

$$H_{\text{eff}} = H_{11} + H_{10}(E - H_{00})^{-1}H_{01} + H_{12}(E - H_{22})^{-1}H_{21}. \tag{2.8}$$

It is clear that the first term in the effective Hamiltonian (2.8) represents the energy for a single electron in the quantum impurity. However, the second and third terms are more subtle. The second term carries information about the influence that the empty state has on the single occupancy, the matrix element H_{10} creates one electron in quantum impurity and annihilates one in the conduction band, and $(E-H_{00})^{-1}$ is the projection of the empty state into the single occupancy. Then, we can conclude that the second term represents the virtual process caused by the presence of the empty state in the single occupation state. Similarly the third represents the virtual process caused by double occupation in the single occupation state.

As discusses above, in the appropriate condition for the Kondo effect to occur, the quantum impurity has a resultant magnetic moment from the unpaired electrons (single occupation state) in the low-energy regime. In this case, the quantum impurity has energy close to the energy for a single occupation state $E \approx E_1 = \varepsilon_d$ and $|\varepsilon_d| > |2\varepsilon_d + U + \langle H_{00}\rangle|, |\langle H_{00}\rangle|$, then $|E| > |\langle H_{22}\rangle|, \langle|H_{00}\rangle|$. Since the terms $(E - H_{00})^{-1}$ and $(E - H_{22})^{-1}$ not commute with H_{10} and H_{12} we need a strategy to solve this. But for now, to simplify the second and third terms of this effective Hamiltonian the familiar geometric series expansion is used,

$$\begin{aligned}(E - H_{00})^{-1} &= \frac{1}{E}\sum_{n=0}^{\infty}\left(\frac{H_{00}}{E}\right)^n, \\ (E - H_{22})^{-1} &= \frac{1}{E}\sum_{n=0}^{\infty}\left(\frac{H_{22}}{E}\right)^n.\end{aligned} \tag{2.9}$$

One way to solve this problem is by transferring all operators from left hand side to right hand side. In case of the term $H_{10}(E - H_{00})^{-1}H_{01}$ (see equation (2.8)) we can transfer all operator in H_{10} to the right, for example. To this end, we write $H_{10}(E-H_{00})^{-1}$ as

$$H_{10}(E - H_{00})^{-1} = \sum_{\mathbf{k}\sigma} V_{\mathbf{k}}(1 - n_{d\bar{\sigma}})d^{\dagger}_{\sigma}c_{\mathbf{k}\sigma}(E - H_{00})^{-1}. \tag{2.10}$$

Note that the operator $c_{\mathbf{k}\sigma}$ does not commute with $(E-H_{00})^{-1}$. We then use the fermionic anticommutation proprieties of the operators and the geometric series defined by (2.9) to

simplify the problem in $c_{\mathbf{k}\sigma}H_{00} = (H_{00} + \varepsilon_{\mathbf{k}})c_{\mathbf{k}\sigma}$. After this, it is easy to show that

$$c_{\mathbf{k}\sigma}(E - H_{00})^{-1} = \frac{1}{\varepsilon_d - \varepsilon_{\mathbf{k}}}\left[1 + \frac{E - H_{00} - \varepsilon_d}{\varepsilon_d - \varepsilon_{\mathbf{k}}}\right]^{-1} c_{\mathbf{k}\sigma}. \tag{2.11}$$

Differently from the previous case, the operator $(1 - n_{d\bar{\sigma}})d^{\dagger}_{\sigma}$ appearing in equation (2.10) commute with H_{00}, so we can transfer this operator directly to the right hand side

$$(1 - n_{d\bar{\sigma}})d^{\dagger}_{\sigma}c_{\mathbf{k}\sigma}(E - H_{00})^{-1} = \frac{1}{\varepsilon_d - \varepsilon_{\mathbf{k}}}\left[1 - \frac{E - H_{00} - \varepsilon_d}{-\varepsilon_d + \varepsilon_{\mathbf{k}}}\right]^{-1} (1 - n_{d\bar{\sigma}})d^{\dagger}_{\sigma}c_{\mathbf{k}\sigma}. \tag{2.12}$$

Putting all the terms together and after some manipulations, we find the complete term in effective Hamiltonian (2.8) that describes the virtual process caused by the presence of the empty state in the single occupancy state as

$$H_{10}(E - H_{00})^{-1}H_{01} = \sum_{\mathbf{k}\mathbf{k}'\sigma\sigma'} \frac{V^{*}_{\mathbf{k}'}V_{\mathbf{k}}}{\varepsilon_d - \varepsilon_{\mathbf{k}}} F(\varepsilon_{\mathbf{k}}, \varepsilon_d) d^{\dagger}_{\sigma}c_{\mathbf{k}\sigma}(1 - n_{d\bar{\sigma}})(1 - n_{d\bar{\sigma}'})c^{\dagger}_{\mathbf{k}'\sigma'}d_{\sigma'}. \tag{2.13}$$

Here we have defined $F(x, y) = \left(1 - \frac{E - H_{00} - \varepsilon_d}{x - y}\right)^{-1}$. This operator $F(x, y)$ itself has no physical meaning and is only inserted here just to simplify the equations.

Similar to the previous case [the second term in effetive Hamiltonian (2.8)], the third term $H_{12}(E - H_{22})^{-1}H_{21}$ can be found by transferring all operator in H_{12} to the right. To do so, we write $H_{12}(E - H_{22})^{-1}$ as

$$H_{12}(E - H_{22})^{-1} = \sum_{\mathbf{k}\sigma} V^{*}_{\mathbf{k}} n_{d\bar{\sigma}} c^{\dagger}_{\mathbf{k}\sigma} d_{\sigma}(E - H_{22})^{-1}. \tag{2.14}$$

The operators $c^{\dagger}_{\mathbf{k}\sigma}$ and d_{σ} not commute with $(E - H_{22})^{-1}$, then we use again the fermionic anticommutation proprieties of the operators and the geometric series defined by (2.9) to simplify the problem in $c^{\dagger}_{\mathbf{k}\sigma}H_{22} = (2\varepsilon_d + U + H_{00} - \varepsilon_{\mathbf{k}})c^{\dagger}_{\mathbf{k}\sigma}n_{d\sigma}n_{d\bar{\sigma}}$. After that and some algebraic manipulations we obtain

$$c^{\dagger}_{\mathbf{k}\sigma}d_{\sigma}(E - H_{22})^{-1} = \frac{1}{\varepsilon_{\mathbf{k}} - \varepsilon_d - U}\left[1 - \frac{E - \varepsilon_d - H_{00}}{\varepsilon_d + U - \varepsilon_{\mathbf{k}}}\right]^{-1} c^{\dagger}_{\mathbf{k}\sigma}d_{\sigma}n_{d\bar{\sigma}}. \tag{2.15}$$

The complete third term in effective Hamiltonian (2.8) that describes the virtual process caused by the presence of the double occupation in the single occupation state is

$$H_{12}(E - H_{22})^{-1}H_{21} = \sum_{\mathbf{k}\mathbf{k}'\sigma\sigma'} \frac{-V^{*}_{\mathbf{k}'}V_{\mathbf{k}}}{\varepsilon_d + U - \varepsilon_{\mathbf{k}'}} F(\varepsilon_d + U, \varepsilon_{\mathbf{k}'}) c^{\dagger}_{\mathbf{k}'\sigma'}d_{\sigma'}n_{d\bar{\sigma}'}n_{d\bar{\sigma}}d^{\dagger}_{\sigma}c_{\mathbf{k}\sigma}, \tag{2.16}$$

where the operator $F(x, y)$ has already been defined.

In the low-energy regime and considering all the previous discussion, the quantum impurity has energy close to the energy for a single occupation state $E \approx \varepsilon_d$, the electrons and holes that participate in the physics of the problem are close to the Fermi level $\varepsilon_{\mathbf{k}} \approx 0$ and $\langle H_{00}\rangle \approx 0$. As the differences in energy are $|\varepsilon_d|, |\varepsilon_d + U| > 0$, in the operator $F(x, y)$, the term $E - \varepsilon_d - H_{00} \approx 0$ which leads to $F(\varepsilon_{\mathbf{k}}, \varepsilon_d), F(\varepsilon_d + U, \varepsilon_{\mathbf{k}'}) \approx 1$.

Another way to solve this same problem is by transferring now all operators from right hand side to left hand side in equation (2.8). In doing this, one have to go through similar algebraic laboring as before. However, we will find small differences with the equations (2.13) and (2.16). Note now that these terms are not Hermitian [(2.13) and (2.16)], and this is a big problem because the effective Hamiltonian must be Hermitian. To overcome this, the symmetrization of the terms in (2.13) and (2.16) are necessary. The procedure to do this is simple, we just do an arithmetic average of the result obtained through the two choices (transfer all operator from right to the left or the opposite). After symmetrizing the second and third complete and Hermitian terms in effective Hamiltonian are found by

$$H_{10}(E-H_{00})^{-1}H_{01} = \sum_{\mathbf{k}\mathbf{k}'\sigma\sigma'} \frac{V^*_{\mathbf{k}'}V_{\mathbf{k}}}{2}\left(\frac{1}{\varepsilon_d-\varepsilon_{\mathbf{k}}}+\frac{1}{\varepsilon_d-\varepsilon_{\mathbf{k}'}}\right) d^\dagger_\sigma c_{\mathbf{k}\sigma}(1-n_{d,\bar{\sigma}})(1-n_{d,\bar{\sigma'}})c^\dagger_{\mathbf{k}'\sigma'}d_{\sigma'}, \tag{2.17}$$

$$H_{12}(E-H_{22})^{-1}H_{21} = \sum_{\mathbf{k}\mathbf{k}'\sigma\sigma'} \frac{-V^*_{\mathbf{k}'}V_{\mathbf{k}}}{2}\left(\frac{1}{\varepsilon_d+U-\varepsilon_{\mathbf{k}}}+\frac{1}{\varepsilon_d+U-\varepsilon_{\mathbf{k}'}}\right) c^\dagger_{\mathbf{k}'\sigma'}d_{\sigma'}n_{d,\bar{\sigma'}}n_{d,\bar{\sigma}}d^\dagger_\sigma c_{\mathbf{k}\sigma}. \tag{2.18}$$

Replacing the equations (2.17) and (2.18) in equation (2.8) we obtain the effective Hamiltonian which captures the essence of the Kondo phenomenon. During the algebraic manipulations we need to pay attention to the terms $n_{d\uparrow}n_{d\downarrow}=0$ and $n_{d\uparrow}+n_{d\downarrow}=1$, since all these calculations are only valid in the regime where the QD is in LM fixed point (single electron in QD with spin $\uparrow$ or $\downarrow$). Is also necessary to define the operators $S^+ = d^\dagger_\uparrow d_\downarrow$, $S^- = d^\dagger_\uparrow d_\downarrow$ and $S^z = \frac{1}{2}(n_{d\uparrow}-n_{d\downarrow})$. After some manipulations we find the effective Hamiltonian by

$$H_{\text{eff}} = H_K + \sum_\sigma \varepsilon_d n_{d\sigma} + \sum_{\mathbf{k}} \frac{|V_{\mathbf{k}}|^2}{\varepsilon_d-\varepsilon_{\mathbf{k}}} + \sum_{\mathbf{k}\mathbf{k}'\sigma} W_{\mathbf{k}\mathbf{k}'}c^\dagger_{\mathbf{k}\sigma}c_{\mathbf{k}'\sigma}, \tag{2.19}$$

where,

$$W_{\mathbf{k}\mathbf{k}'} = -\frac{V^*_{\mathbf{k}'}V_{\mathbf{k}}}{4}\left(\frac{1}{\varepsilon_d-\varepsilon_{\mathbf{k}}}+\frac{1}{\varepsilon_d-\varepsilon_{\mathbf{k}'}}+\frac{1}{\varepsilon_d+U-\varepsilon_{\mathbf{k}}}+\frac{1}{\varepsilon_d+U-\varepsilon_{\mathbf{k}'}}\right), \tag{2.20}$$

The first term above is the Kondo Hamiltonian [see equation (2.3)]. It is easy to understand that the first term is exactly the Kondo Hamiltonian, since it was used to explain the phenomenon for the first time and works well. The second and third terms in effective Hamiltonian (2.19), only re-scale the reference energy, and the last term in effective Hamiltonian are scattering potentials, then this terms do not have any importance in the scaling procedure since the main physics of the problem is within the Kondo Hamiltonian H_K.

In addition, we find the effective coupling $J_{\mathbf{kk'}}$ in function of ε_d, U and $V_{\mathbf{k}}$. The term $V_{\mathbf{k}}$ is what in Anderson's model connects the electrons in the conduction band to impurity. This term is localized, assuming that the conducting electrons couples to the impurity very close to it, thus in the $\mathbf{k}$-space it is approximately constant. Remember that all this analysis are valid at low energies so that the energy of the conduction electrons are close to the Fermi level ($|\varepsilon_d| \gg \varepsilon_{\mathbf{k}}, \varepsilon_{\mathbf{k'}}$ and $\varepsilon_d + U \gg \varepsilon_{\mathbf{k}}, \varepsilon_{\mathbf{k'}}$). With this in mind, we can write

$$\begin{aligned} J_{\mathbf{kk'}} &= \frac{V_{\mathbf{k'}}^* V_{\mathbf{k}}}{2}\left(-\frac{1}{\varepsilon_d - \varepsilon_{\mathbf{k}}} - \frac{1}{\varepsilon_d - \varepsilon_{\mathbf{k'}}} + \frac{1}{\varepsilon_d + U - \varepsilon_{\mathbf{k}}} + \frac{1}{\varepsilon_d + U - \varepsilon_{\mathbf{k'}}}\right), \\ &\simeq |V|^2\left(-\frac{1}{\varepsilon_d} + \frac{1}{\varepsilon_d + U}\right) = J. \end{aligned} \tag{2.21}$$

Within the conditions described in the previous paragraph, we can write the scattering potential term $W_{\mathbf{kk'}}$ as

$$W_{\mathbf{kk'}} = W \simeq \frac{|V|^2}{2}\left(\frac{1}{\varepsilon_d} + \frac{1}{\varepsilon_d + U}\right). \tag{2.22}$$

In the particle-hole symmetry $\varepsilon_d = -U/2$, observe that this term vanishes. Thus, within the scope of this work, even considering the scattering potential, this term does not contribute to the physics of the problem.

Now that we have the models at hand, we can use the poor man's scaling analyses to obtain the behavior of the effective parameters (scaling equations), for the Anderson Model or the Kondo Hamiltonian. These scale equations will give us valuable information about the behavior of the system magnetic impurity and conduction band in certain regimes. Some of this information is the Kondo temperature T_K and the critical coupling J_C.

3 Some theoretical approaches to the Anderson and Kondo models

3.1 Poor man's scaling

In physics, most of the know phenomena occur at some specific energy scales. In other words, the phenomena are commonly described adequately within certain important energy ranges, so that processes involving other energy scales can be safely discarded. This is not always the case, the Kondo problem is one example in which all energy scale matter. We are then interested in processes occurring at low energy regime, but are affected by all the energy scales of the problem. The question is how to get there from the model formulated in high energy scales. The main idea is that, instead of giving importance to the fine details of the high energy model, one can reach the properties at low energies by monitoring the behavior of the system by slowly reducing the energy scale. This idea of elucidating the low-energy universal behavior is achieved by the so-called renormalization group procedure, which consists of two steps [see [57] and figure 5 to the Poor man's scaling general ideas]:

- 1- Rescale the energy cutoff $\Lambda \to \Lambda/b$, where $b > 1$, and integrate out the degrees of freedom in the energy range. This will result in the change of the Hamiltonian $H(\Lambda) \to H'$
- 2- Rescale the energy scales back so that $E = bE'$ and the new Hamiltonian $H(\Lambda/b) \to bH'$.

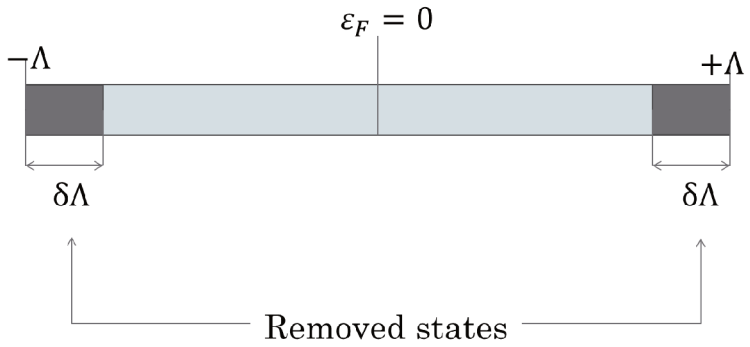

Figure 5 – Representation of the energy scale and general idea to Poor man's scaling. High energy states are removed and considered in a pertubative way.

Following the idea of the renormalization group discussed above we will discuss how to eliminate the high energy states of the system. The way is to integrate on the corresponding degrees of freedom whose energy lie within an interval $\Lambda \in [D - \delta\Lambda, D]$. The Hamiltonian will depend on the energy scale $D - \delta\Lambda$ and will take the form $H(\Lambda)$, with the effective parameters. In particular for Poor man's scaling, after removing the high energy states, the Hamiltonian is not re-scaled back to the initial scale.

3.1.1 Poor man's scaling in Kondo Hamiltonian

In 1970 Phillip Anderson derived an approache called Poor Man's Scaling, which consists of eliminating in a pertubative mode the high energy excitations [58]. For simplicity we use the effective Hamiltonian (2.19), deduced for QD coupled with just one lead. The effective Hamiltonian found has four terms. Note that with the exception of the first term, all others do not cause spin-flip (scattering mechanism relevant to the Kondo effect). Thus, they represent only potential scattering or an overall shift of the reference energy and do not renormalize the term of coupling that we are interested in. Then, for this work we will consider only the Kondo Hamiltonian term in effective Hamiltonian $H = H_K$ to the Poor man's scaling analysis.

Following Anderson's idea, we eliminate high-energy fluctuations using the scattering matrix formalism (T-matrix), which describes the scattering of an electron from an initial state $|\mathbf{k}\sigma\rangle$ in a final state $|\mathbf{k}'\sigma'\rangle$. The scattering matrix as a function of energy can be written up to in second order as,

$$T(E) = \sum_{\mathbf{k},\mathbf{k}'} \left(H_{\mathbf{k},\mathbf{k}'} + \sum_{\boldsymbol{q}\in\ \{\varepsilon_{\boldsymbol{q}} \ll 0\}} H_{\mathbf{k},\boldsymbol{q}}(E - H_0)^{-1} H_{\boldsymbol{q},\mathbf{k}'} + \sum_{\boldsymbol{q}\in\ \{\varepsilon_{\boldsymbol{q}} \gg 0\}} H_{\boldsymbol{q},\mathbf{k}'}(E - H_0)^{-1} H_{\mathbf{k},\boldsymbol{q}} \right), \tag{3.1}$$

where $H_{\mathbf{k},\mathbf{k}'}$ represents each term of the effective Hamiltonian. $\varepsilon_{\boldsymbol{q}}$ is the energy associated with the quasi-momentum vector $\boldsymbol{q}$ of the high-energy electrons. If $\varepsilon_{\boldsymbol{q}} \gg 0$ then the energy level is far above the Fermi level (the empty state state is most probable $n_{\boldsymbol{q}\sigma} = 0$), in the opposite case it is far below ε_F (the double occupancy state is most probable $n_{\boldsymbol{q}\sigma} = 1$).

The second term in T-matrix describes the hole-type scattering within the high-energy sector of the Hilbert space and the third term the particle-type scattering within the high energy sector. These scattering processes are represented in figure 6. In figure 6(a) an initial particle state $|\mathbf{k}\sigma\rangle$ scatter into the impurity spin represented by the letter A (S^+, S^- or S^z) and then propagates to the second scattering in the impurity spin represented by the letter B (S^+, S^- or S^z) and leaves with a final state $|\mathbf{k}'\sigma'\rangle$. Figure 6 (b) represents hole-type scattering. In this case, we have an electron in a state that can be scattered with spin-flip for a final state $|\mathbf{k}'\sigma'\rangle$ and a hole remaining that will be annihilated by an initial state $|\mathbf{k}\sigma\rangle$.

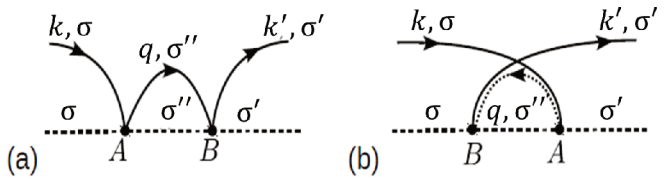

Figure 6 – Feynman diagrams representing the contributions up to second-order scattering processes for the general case. (a) represents scattering of the particle-type. An initial particle state $|\mathbf{k}\sigma\rangle$ scatter into the impurity spin and leaves with a final state $|\mathbf{k}'\sigma'\rangle$. (b) represents hole-type scattering. In this case, we have an electron in a state that can be scattered with spin-flip for a final state $|\mathbf{k}'\sigma'\rangle$ and a hole remaining that will be annihilated by an initial state $|\mathbf{k}\sigma\rangle$. Figure adapted from [2].

One strategy to solve the scattering matrix [T-matrix in (3.2)] is to use series expansion in the term $(E - H_0)^{-1}$ and transfer all operators from the left side to the right of that term, as was done previously. The same considerations to simplify the terms were also used, then we can written the T-matrix

$$T(E) = H_K + \sum_{\mathbf{k},\mathbf{k}'} \left(\sum_{q \in \{\varepsilon_q \ll 0\}} \frac{1}{\varepsilon_{\mathbf{k}} - \varepsilon_q} H_{\mathbf{k},q} H_{q,\mathbf{k}'} + \sum_{q \in \{\varepsilon_q \gg 0\}} \frac{1}{\varepsilon_q - \varepsilon_{\mathbf{k}}} H_{q,\mathbf{k}'} H_{\mathbf{k},q} \right). \tag{3.2}$$

After a very long algebraic manipulations the equation becomes as

$$T(E) = H_K \left(1 - 2J \sum_q \frac{1}{\varepsilon_q} \right) = H_K \left(1 + \frac{\delta J}{J} \right), \tag{3.3}$$

where we have conveniently defined

$$\delta J = -2J^2 \sum_q \frac{1}{\varepsilon_q}. \tag{3.4}$$

The equation above is the simplified version of the T-matrix, after taking into account all the considerations already mentioned, and also considering the conduction electrons is close to the Fermi level ($\varepsilon_{\mathbf{k}}, \varepsilon_{\mathbf{k}'} \approx 0$ and $|\varepsilon_q| \gg 0$). Note that the scattering matrix has the same form of the Kondo Hamiltonian H_K, but with a difference in the coupling term δJ. The term δJ represents the change in the effective coupling term that the Hamiltonian acquires when a small piece at the extremities of the conduction band is removed.

To find the equation for the effective coupling we must sum over all degrees of freedom $\boldsymbol{q}$. This can be done by integrating (change the variable $\varepsilon_q \to \Lambda$) over this small piece of the conduction band $[\Lambda - \delta\Lambda, \Lambda]$, and multiplying by the density of states $\rho(\Lambda)$. As a result, we obtain

$$\frac{\delta J}{\delta \ln \Lambda} = -2\rho(\Lambda) J^2, \tag{3.5}$$

which is called the β-equation [equation (3.5)]. In the limit that $\delta \to 0$ then δ can be replaced in the equation by d and we can use the mathematical tools of Calculus.

One of the fixed points of the Hamiltonian in the Kondo problem is called the strong coupling limit and happens when the coupling term diverges ($J \to \infty$). In this case, the impurity forms a singlet with the electrons of the conduction band and the Kondo effect occurs. To find this fixed point we must integrate the β-equation in the direction of the high energies for low energies to the point where the coupling diverges ($J(\Lambda^*) \to \infty$). At this point, we can estimate the Kondo temperature by $\Lambda^* \sim T_K$.

The simplest case is for a flat conduction band $\rho(\Lambda) = 1/2D$, upon integrating the β-equation from D a lower limit Λ^* where $J(\Lambda^*) \to \infty$, we find the estimate for T_k

$$T_K \sim De^{-\frac{D}{J_0}}. \tag{3.6}$$

In particle-hole symmetry $\rho_0 J_0 = \frac{4\Gamma_0}{\pi U}$ (see equation (2.21)) and for metallic conductor (flat band) $\rho_0 = \frac{1}{2D}$, then this equation can be written by

$$T_K \sim De^{-\frac{\pi U}{8\Gamma_0}}. \tag{3.7}$$

This equation is very similar to the one deduced by Haldane in 1978 [59]. In Haldane's work, he finds an estimate of T_K using a scaling procedure in the asymmetric Anderson Model. Something remarkable is that the procedure used is very close to the poor man's scaling in the Anderson Model that will be shown in subsection 3.1.3. Within more general considerations, Haldane arrived that T_K can be estimated by

$$T_K \sim D\sqrt{\frac{U\Gamma_0}{2}}e^{-\frac{\pi U}{8\Gamma_0}}. \tag{3.8}$$

We could come to a conclusion close to Haldane's if we use the scattering matrix (T-matrix) in third order, but that is not the focus of this work.

3.1.2 PMS example: Pseudo-gap systems

Pseudo-gap or gapless are systems that exhibit a particular behavior where the gap between conduction and valence band is zero. As already mentioned, the density of states has the general form $\rho(\Lambda) = \rho_0|\Lambda|^r$, where $\rho_0 = \frac{(r+1)}{2D^{r+1}}$ is the normalization factor. As an example the application of the poor man's scaling, we want to briefly explore the physics of a magnetic impurity coupled to this type of conduction band. Within this approach we can estimate, for instance, the Kondo temperature T_K (similar to the previous one with the flat band) and also the critical coupling J_C below which no Kondo screening is possible.

In analogy to the case of the flat band we start from the β-equation (3.5) and replacing the pseudo-gap density of states $\rho_0|\Lambda|^r$, upon which we find the differential equation for J as

$$-\frac{dJ}{J^2} = 2\rho_0\Lambda^{r-1}d\Lambda. \tag{3.9}$$

We can solve this equation by direct integration in the range $\Lambda^* \leq \Lambda \leq D$ with the initial condition $J(D) = J_0$,

$$\left(\frac{1}{J(\Lambda^*)} - \frac{1}{J_0}\right) = 2\rho_0 \int_D^{\Lambda^*} \Lambda^{r-1}d\Lambda = \frac{2\rho_0}{r}[\Lambda^{*r} - D^r]. \tag{3.10}$$

Again, in the Kondo regime the coupling term diverges $[J(\Lambda^*) \to \infty]$, a condition that provides us with Λ^*. Remembering that this quantity is usually taken as T_K, then we estimate the Kondo temperature for pseudo-gap as

$$T_K \sim \Lambda^* = D\left[1 - \frac{r}{r+1}\frac{D}{J_0}\right]^{\frac{1}{r}}. \tag{3.11}$$

Besides that, it is not difficult to show that at the limit $r \to 0$, this equation becomes the equation deduced for the metallic flat band (3.6).

Imposing the condition that Λ^* must be within the region defined by finite density of states (since without electrons in the conduction band the are no strong coupling limit), something curious happens: this condition leads to a restriction in the values of J_0 for the Kondo effect to occur, namely

$$0 < \Lambda^* < D \Leftrightarrow J_0 > J_C = \frac{rD}{r+1}. \tag{3.12}$$

We can write this result in another way. Defining $\rho_0' = D^r\rho_0$, we can show that $2\rho_0' J_C = r$, and this result is already known in the literature for pseudo-gap systems [see [32] for more details about this system].

3.1.3 Poor man's scaling analysis to the Anderson Model

Following Cheng *et al.* [32], we perform a poor man's scaling calculation on our H_{SIAM}. Application of the poor man's scaling to Anderson Model is similar but has small differences than the Poor man's scaling calculations to the Kondo model. Now, the strategy to find the renormalized parameters of the Anderson Model (2.2) $\tilde{U}$, $\tilde{V}_{\mathbf{k}}$ and $\tilde{\varepsilon}_d$ is to use second order non-degenerate perturbation theory. We start with the many body stats in simplified notation for the many-body states (number of the electrons in quantum impurity) $|0\rangle$, $|1_\sigma\rangle = d_\sigma^\dagger|0\rangle$ and $|2\rangle = d_\sigma^\dagger d_{\bar{\sigma}}^\dagger|0\rangle$. However, the many-body state in it's complete form is

$$|n_{d\uparrow} + n_{d\downarrow}; ...n_{\mathbf{k}\sigma}...\rangle, \tag{3.13}$$

where $n_{\mathbf{k}\sigma}$ is the number of electrons in conduction band with energy $\varepsilon_{\mathbf{k}}$ and spin σ. Without losing any information, the Anderson model (2.2) can be separated into two terms H_0 and H' where

$$H_0 = \sum_\sigma \left(\varepsilon_d n_{d\sigma} + \frac{U}{2} n_{d\sigma} n_{d\bar{\sigma}}\right) + \sum_{\mathbf{k}\sigma} \varepsilon_{\mathbf{k}} n_{\mathbf{k}\sigma}, \tag{3.14}$$

describes the impurity and conduction band decoupled from each other and is diagonal on the chosen base ($|n_{d\uparrow} + n_{d\downarrow}; ...n_{\mathbf{k}\sigma}...\rangle$). In this procedure the pertubative term H' is the hybridization term in Anderson Model (2.2),

$$H' = \sum_{\mathbf{k}\sigma} V_{\mathbf{k}} d_\sigma^\dagger c_{\mathbf{k}\sigma} + V_{\mathbf{k}}^* c_{\mathbf{k}\sigma}^\dagger d_\sigma. \tag{3.15}$$

Before proceeding with the calculations let us brief discuss some basic properties of the Hamiltonian H_0. This Hamiltonian is basically the sum of the impurity energy and the conduction band. As such, at temperature $T = 0$, the conduction band states with energy below the Fermi level ($\varepsilon_F = 0$) are completely filled and the conduction band states with energy above are completely empty (this is the ground state of the conduction band Hamiltonian). The energy for the quantum impurity levels has already been discussed and herewith the conduction band we can conclude that the many body state at zero temperature together with their energies are

$$\begin{aligned} |0\rangle^{(0)} \quad &\Rightarrow E_0^{(0)} = \left\langle \left(\sum_{\mathbf{k}\sigma} \varepsilon_{\mathbf{k}} n_{\mathbf{k}\sigma}\right)_{T=0} \right\rangle, \\ |1_\sigma\rangle^{(0)} \quad &\Rightarrow E_1^{(0)} = E_0^{(0)} + \varepsilon_d, \\ |2\rangle^{(0)} \quad &\Rightarrow E_2^{(0)} = E_0^{(0)} + 2\varepsilon_d + U. \end{aligned} \tag{3.16}$$

At this point it is useful to define the vector $\mathbf{k}^-$ for the electrons with energy $\varepsilon_{\mathbf{k}^-} < \varepsilon_F$ and the vector $\mathbf{k}^+$ for the electrons with energy $\varepsilon_{\mathbf{k}^+} > \varepsilon_F$.

In second order non-degenerate perturbation theory the state $|m\rangle$ with energy E_m is changed to the state $|\tilde{m}\rangle$ with energy $\tilde{E}_m$ due to the presence of the perturbative term

H'.

$$\begin{aligned} |\tilde{m}\rangle &= |m\rangle + \sum_{n\neq m} \frac{\langle n|H'|m\rangle}{E_m - E_n}|n\rangle + O(V^2). \\ \tilde{E}_m &= E_m + \langle m|H'|m\rangle + \sum_{n\neq m} \frac{|\langle n|H'|m\rangle|^2}{E_m - E_n} + O(V^3). \end{aligned} \tag{3.17}$$

The idea is to use the same concepts in the Anderson Model ($H_0 + H'$) on the basis defined by (3.13) to find the many body states ($|0\rangle$, $|1_\sigma\rangle$ and $|2\rangle$) corrected by the presence of the coupling between the quantum impurity and the conduction band.

We start the calculations with the empty state $|0\rangle$. In Anderson Model, the empty state subspace is not connected to the dual occupation subspace, since in the Anderson Hamiltonian the quantum impurity can exchange only one electron at a time with the conduction band. Thus, using (3.17) to empty state we can find the term corrected by the pertubative term $|\tilde{0}\rangle$,

$$\begin{aligned} |\tilde{0}\rangle &= |0\rangle^{(0)} + \sum_{\sigma} \sum_{\sigma''\{n_{\mathbf{k}\sigma''}\}} \frac{\langle 1_\sigma|H'|0\rangle^{(0)}}{E_0^{(0)} - E_1}|1_\sigma\rangle + O(V^2), \\ &= |0\rangle^{(0)} + \sum_{\sigma} \sum_{\sigma''\{n_{\mathbf{k}\sigma''}\}} \sum_{\sigma'\{n_{\mathbf{k}'\sigma'}\}} -V_{\mathbf{k}} \frac{\langle 1_\sigma|c_{\mathbf{k}'\sigma'}|1_{\sigma'}\rangle^{(0)}}{E_0^{(0)} - E_1}|1_\sigma\rangle + O(V^2). \end{aligned} \tag{3.18}$$

Note that a sum in the occupancy number for the conduction electrons ($\{n_{\mathbf{k}\sigma''}\}$) has been added. This is necessary since any combination of the distribution in the conduction band is an eigenstate of the H_0. One should not forget that, at zero temperature the conduction band levels above the Fermi level are completely empty so $c_{\mathbf{k}'\sigma'}|1_{\sigma'}\rangle^{(0)}$ annihilates one electron in the state $\mathbf{k}'$ with spin σ'

$$\begin{aligned} |\tilde{0}\rangle &= |0\rangle^{(0)} + \sum_{\sigma} \sum_{\sigma''\{n_{\mathbf{k}\sigma''}\}} \sum_{\sigma'\{n_{\mathbf{k}'\sigma'}\}} -V_{\mathbf{k}} \frac{\langle 1_\sigma, ...n_{\mathbf{k}\sigma''}...|1_{\sigma'}, ...n_{\mathbf{k}'\sigma'} - 1...\rangle}{E_0^{(0)} - E_1}|1_\sigma, ...n_{\mathbf{k}\sigma''}...\rangle + O(V^2), \\ &= |0\rangle^{(0)} + \sum_{\sigma} \sum_{\sigma''\{n_{\mathbf{k}\sigma''}\}} \sum_{\sigma'\{n_{\mathbf{k}'\sigma'}\}} \frac{-V_{\mathbf{k}}\delta_{\sigma,\sigma'}\delta_{\sigma'',\sigma'}\delta_{n_{\sigma\mathbf{k}},(n_{\sigma'\mathbf{k}'}-1)}}{E_0^{(0)} - (E_1^{(0)} + |\varepsilon_{\mathbf{k}}|)} c_{\mathbf{k}\sigma}|1_\sigma\rangle^{(0)} + O(V^2), \end{aligned} \tag{3.19}$$

then only electrons with $\mathbf{k}' \in \mathbf{k}^-$ contribute to this expression above. After replacing the sum in $\{n_{\mathbf{k}\sigma''}\}$ for $\mathbf{k}$ we can finally write the state $|\tilde{0}\rangle$ as

$$|\tilde{0}\rangle = |0\rangle^{(0)} + \sum_{\sigma,\mathbf{k}\in\mathbf{k}^-} \frac{V_{\mathbf{k}}}{\varepsilon_d + |\varepsilon_{\mathbf{k}}|} c_{\mathbf{k}\sigma}|\sigma\rangle^{(0)} + O(V^2). \tag{3.20}$$

The energy of this state $\tilde{E}_0$ can also be found through the procedure described in (3.17) using second order pertubation theory. As has already been discussed, the empty subspace is only coupled with the single occupancy subspace, so the corrected energy $\tilde{E}_0$ can be written as

$$\begin{aligned} \tilde{E}_0 &= E_0^{(0)} + \sum_{\sigma} \sum_{\sigma''\{n_{\mathbf{k}\sigma''}\}} \frac{|\langle 1_\sigma|H'|0\rangle^{(0)}|^2}{E_0^{(0)} - E_1} + O(V^3), \\ &= E_0^{(0)} + \sum_{\sigma} \sum_{\sigma''\{n_{\mathbf{k}\sigma''}\}} \frac{(\langle 1_\sigma|H'|0\rangle^{(0)})(\langle 1_\sigma|H'|0\rangle^{(0)})^*}{E_0^{(0)} - E_1} + O(V^3). \end{aligned} \tag{3.21}$$

Observe now that the term $\langle 1_\sigma|H'|0\rangle^{(0)}$ has already been resolved. We can then use this to obtain

$$\tilde{E}_0 = E_0^{(0)} - 2\sum_{\mathbf{k}\in\mathbf{k}^-}\frac{|V_\mathbf{k}|^2}{\varepsilon_d + |\varepsilon_\mathbf{k}|} + O(V^3). \tag{3.22}$$

Unlike $|0\rangle$ and $|2\rangle$, the single occupancy state $|1_\sigma\rangle$ is connected to the empty state and the dual occupation state. These calculations are very similar to those performed previously for state $|0\rangle$, so less details will be shown for the next ones. As in the previous case, using (3.17) to the single occupation state we can find the corrected state $|\tilde{1}_\sigma\rangle$ by

$$\begin{aligned}|\tilde{1}_\sigma\rangle &= |1_\sigma\rangle^{(0)} + \sum_{\sigma''\{n_{\mathbf{k}\sigma''}\}}\frac{\langle 0|H'|1_\sigma\rangle^{(0)}}{E_1^{(0)} - E_0}|0\rangle + \sum_{\sigma''\{n_{\mathbf{k}\sigma''}\}}\frac{\langle 2|H'|1_\sigma\rangle^{(0)}}{E_1^{(0)} - E_2}|2\rangle + O(V^2),\\ &= |1_\sigma\rangle^{(0)} + \sum_{\sigma''\{n_{\mathbf{k}\sigma''}\}}\sum_{\sigma'\{n_{\mathbf{k}'\sigma'}\}}\frac{V_\mathbf{k}^*\langle 0|c_{\mathbf{k}'\sigma'}^\dagger|0\rangle^{(0)}}{E_1^{(0)} - E_0}|0\rangle - \sum_{\sigma''\{n_{\mathbf{k}\sigma''}\}}\sum_{\sigma'\{n_{\mathbf{k}'\sigma'}\}}\frac{\sigma V_\mathbf{k}\langle 2|c_{\mathbf{k}'\overline{\sigma'}}|2\rangle^{(0)}}{E_1^{(0)} - E_2}|2\rangle + O(V^2).\end{aligned} \tag{3.23}$$

As previously discussed at zero temperature the conduction band are completely empty above the Fermi level and below are completely filled. The term $c_{\mathbf{k}'\sigma'}^\dagger|0\rangle^{(0)}$ create one electron in the conduction state $\mathbf{k}'$ with spin σ'. But an electron can only be created if this state are empty by the Pauli exclusion principle. As a result, in the first term only electrons with $\mathbf{k}' \in \mathbf{k}^+$ contribute to this calculation. The term $c_{\mathbf{k}'\overline{\sigma'}}|2\rangle^{(0)}$ annihilates one electron in the conduction state $\mathbf{k}'$ with spin $\overline{\sigma'}$, but this state must have electrons to be annihilated. Therefore, in the second term only electrons with $\mathbf{k}' \in \mathbf{k}^-$ contribute. After this considerations and some math manipulations we can write the state $|\tilde{1}_\sigma\rangle$ as

$$|\tilde{1}_\sigma\rangle = |1_\sigma\rangle^{(0)} + \sum_{\mathbf{k}\in\mathbf{k}^+}\frac{V_\mathbf{k}^*}{\varepsilon_d - |\varepsilon_\mathbf{k}|}c_{\mathbf{k}\sigma}^\dagger|0\rangle^{(0)} + \sum_{\mathbf{k}\in\mathbf{k}^-}\frac{\sigma V_\mathbf{k}}{\varepsilon_d + U + |\varepsilon_\mathbf{k}|}c_{\mathbf{k}\sigma}|2\rangle^{(0)} + O(V^2). \tag{3.24}$$

The energy of this state $\tilde{E}_1$, again, using (3.17), can be written as

$$\tilde{E}_1 = E_0^{(0)} + \varepsilon_d + \sum_{\mathbf{k}\in\mathbf{k}^+}\frac{|V_\mathbf{k}|^2}{\varepsilon_d - |\varepsilon_\mathbf{k}|} - \sum_{\mathbf{k}\in\mathbf{k}^-}\frac{|V_\mathbf{k}|^2}{\varepsilon_d + U + |\varepsilon_\mathbf{k}|} + O(V^3). \tag{3.25}$$

Alike the empty state, the dual occupation state $|2\rangle$ is not connected to the empty state subspace. Then using (3.17), we can find the corrected state $|\tilde{2}\rangle$

$$\begin{aligned}|\tilde{2}\rangle &= |2\rangle^{(0)} + \sum_\sigma\sum_{\sigma''\{n_{\mathbf{k}\sigma''}\}}\frac{\langle 1_\sigma|H'|2\rangle^{(0)}}{E_2^{(0)} - E_1}|1_\sigma\rangle + O(V^2),\\ &= |2\rangle^{(0)} + \sum_\sigma\sum_{\sigma''\{n_{\mathbf{k}\sigma''}\}}\sum_{\sigma'\{n_{\mathbf{k}'\sigma'}\}}\frac{\overline{\sigma'}V_{\mathbf{k}'}^*\langle 1_\sigma|c_{\mathbf{k}'\overline{\sigma'}}^\dagger|1_{\sigma'}\rangle^{(0)}}{E_2^{(0)} - E_1}|1_\sigma\rangle + O(V^2).\end{aligned} \tag{3.26}$$

The term $c_{\mathbf{k}'\overline{\sigma'}}^\dagger|0\rangle^{(0)}$ create one electron in the conduction state $\mathbf{k}'$ with spin $\overline{\sigma'}$. But an electron can only be created if this state are empty by the Pauli exclusion principle.Then, at zero temperature, only electrons with $\mathbf{k}' \in \mathbf{k}^+$ contribute to this calculation. From these

considerations we can write the state $|\tilde{2}\rangle$ by

$$|\tilde{2}\rangle = |2\rangle^{(0)} + \sum_{\sigma,\mathbf{k}\in\mathbf{k}^+} \frac{\overline{\sigma}V_{\mathbf{k}}^*}{\varepsilon_d + U - |\varepsilon_{\mathbf{k}}|} c_{\mathbf{k}\overline{\sigma}}^\dagger |1_\sigma\rangle^{(0)} + O(V^2), \tag{3.27}$$

while the energy $\tilde{E}_2$ can be written as

$$\tilde{E}_2 = E_0^{(0)} + 2\varepsilon_d + U - 2\sum_{\sigma,\mathbf{k}\in\mathbf{k}^+} \frac{|V_{\mathbf{k}}|^2}{\varepsilon_d + U - |\varepsilon_{\mathbf{k}}|} + O(V^3). \tag{3.28}$$

Now we have the corrected states $|\tilde{0}\rangle$, $|\tilde{1}_\sigma\rangle$ and $|\tilde{2}\rangle$ and the energies corrected $\tilde{E}_0$, $\tilde{E}_1$ and $\tilde{E}_2$. We a ready to derive the scaling equations for the effective parameters $\tilde{U}$, $\tilde{\varepsilon}_d$ and $\tilde{V}_{\mathbf{k}}$. For the last, the scaling equation shows that $\tilde{V}_{\mathbf{k}} = V_{\mathbf{k}} + O(V^3)$ [see Ref. [32]]. The differences in energy levels for impurity have been discussed previously in the section 2.1, so we know that the energy difference between the single occupation and empty state is $\tilde{E}_1 - \tilde{E}_0 = \tilde{\varepsilon}_d$. In addiction the difference between the dual occupation and the single occupation states is $\tilde{E}_2 - \tilde{E}_1 = \tilde{\varepsilon}_d + \tilde{U}$. Using the equations (3.22), (3.25) and (3.28) we find

$$\tilde{\varepsilon}_d \approx \varepsilon_d - \sum_{\mathbf{k}\in\mathbf{k}^+} \frac{|V_{\mathbf{k}}|^2}{-\varepsilon_d + |\varepsilon_{\mathbf{k}}|} - \sum_{\mathbf{k}\in\mathbf{k}^-} \frac{|V_{\mathbf{k}}|^2}{\varepsilon_d + U + |\varepsilon_{\mathbf{k}}|} + 2\sum_{\mathbf{k}\in\mathbf{k}^-} \frac{|V_{\mathbf{k}}|^2}{\varepsilon_d + |\varepsilon_{\mathbf{k}}|}, \tag{3.29}$$

and

$$\tilde{U} \approx U + 2\left[\sum_{\mathbf{k}\in\mathbf{k}^+} \frac{|V_{\mathbf{k}}|^2}{-\varepsilon_d + |\varepsilon_{\mathbf{k}}|} - \sum_{\mathbf{k}\in\mathbf{k}^+} \frac{|V_{\mathbf{k}}|^2}{\varepsilon_d + U - |\varepsilon_{\mathbf{k}}|} - \sum_{\mathbf{k}\in\mathbf{k}^-} \frac{|V_{\mathbf{k}}|^2}{\varepsilon_d + |\varepsilon_{\mathbf{k}}|} + \sum_{\mathbf{k}\in\mathbf{k}^-} \frac{|V_{\mathbf{k}}|^2}{\varepsilon_d + U + |\varepsilon_{\mathbf{k}}|}\right]. \tag{3.30}$$

Where $\tilde{\varepsilon}_d$ is the effective energy for one electron in quantum impurity and $\tilde{U}$ is the effective Coulomb repulsion.

The next step is re-scaling the equations (3.29) and (3.30) as described in Figure 5. For a small piece of the conduction band removed $|\delta\Lambda| = D - \Lambda$ the summations can be approximated by $\sum_{\mathbf{k}\in\mathbf{k}^+} g(\varepsilon_{\mathbf{k}}) \approx g(\Lambda)\rho(\Lambda)\delta\Lambda$ and $\sum_{\mathbf{k}\in\mathbf{k}^-} g(\varepsilon_{\mathbf{k}}) \approx g(-\Lambda)\rho(-\Lambda)\delta\Lambda$ where Λ is the new bandwidth. Assuming $V_{\mathbf{k}}$ real and $\mathbf{k}$-independent $V_{\mathbf{k}} \approx V$, we can rewrite the above equations as

$$\tilde{\varepsilon}_d - \varepsilon_d \approx -\left[\frac{\rho(\Lambda)|V|^2}{-\varepsilon_d + \Lambda} - \frac{\rho(-\Lambda)|V|^2}{\varepsilon_d + U + \Lambda} + 2\frac{\rho(-\Lambda)|V|^2}{\varepsilon_d + \Lambda}\right]\delta\Lambda, \tag{3.31}$$

and

$$\tilde{U} - U \approx 2\left[\frac{\rho(\Lambda)|V|^2}{-\varepsilon_d + \Lambda} - \frac{\rho(\Lambda)|V|^2}{\varepsilon_d + U - \Lambda} - \frac{\rho(-\Lambda)|V|^2}{\varepsilon_d + \Lambda} + \frac{\rho(-\Lambda)|V|^2}{\varepsilon_d + U + \Lambda}\right]\delta\Lambda. \tag{3.32}$$

When removing a second piece of the conduction band, the previous equations are re-scaling by replacing $\varepsilon_d \to \tilde{\varepsilon}_d$, $U \to \tilde{U}$, $\tilde{\varepsilon}_d \to \tilde{\varepsilon}_d - \delta\tilde{\varepsilon}_d$ and $\tilde{U} \to \tilde{U} - \delta\tilde{U}$. For simplicity, we can insert the hybridization function $\Gamma(\Lambda) = \pi|V|^2\rho(\Lambda)$ we find

$$\frac{\delta\tilde{\varepsilon}_d}{\delta\Lambda} = \frac{1}{\pi}\left[\frac{\Gamma(\Lambda)}{\Lambda - \tilde{\varepsilon}_d} + \frac{\Gamma(-\Lambda)}{\Lambda + \tilde{\varepsilon}_d + \tilde{U}} - 2\frac{\Gamma(-\Lambda)}{\Lambda + \tilde{\varepsilon}_d}\right], \tag{3.33}$$

and

$$\frac{\delta\tilde{U}}{\delta\Lambda} = \frac{2}{\pi}\left[-\frac{\Gamma(\Lambda)}{\Lambda - \tilde{\varepsilon}_d} + \frac{\Gamma(\Lambda)}{\Lambda - \tilde{\varepsilon}_d - \tilde{U}} + \frac{\Gamma(-\Lambda)}{\Lambda + \tilde{\varepsilon}_d} - \frac{\Gamma(-\Lambda)}{\Lambda + \tilde{U} + \tilde{\varepsilon}_d}\right]. \tag{3.34}$$

At this point we have the scaling equations for the renormalized parameters, J for the Kondo Hamiltonian and $\tilde{U}$, $\tilde{\varepsilon}_d$, $\tilde{\Gamma}$ obtained through the poor man's scaling procedure. In the next chapter we will apply these scaling equations to the main problem of a magnetic impurity coupled to a gapped band, which we are interested in.

3.2 Numerical renormalization group

Poor man's scaling is a very useful approach to obtain certain properties of the system at energy scales larger than the Kondo temperature. Beyond that point, the effective coupling constant diverges and the theoretical predictions cannot be trusted. Therefore, we need another method to obtain information below the Kondo temperature scale. Numerical Renormalization Group [NRG, created by Kenneth G. Wilson in the 1970s [6]] is a convenient method that allow us to investigate the renormalization flow to energy scale down to the Fermi level. The basic ideas of NRG [see Refs. [60, 61, 62, 63] for more details] can be summarized in the following six steps below:

- 1- Logarithmic division of the conduction band. This was the first step in the derivation and the most important one, allows handling the logarithmic divergence mentioned in The Kondo Effect. The conduction band is split into intervals that decrease towards low energies: $\pm[\Lambda^{-n-1}, \Lambda^{-n}]$, where $\Lambda > 1$ and n is an integer>=0.

- 2 - Fourier expansion of each interval, using orthogonal basis functions that are zero outside the interval.

- 3 - Approximating the impurity orbital by using only the Wannier orbital centered on the impurity. It turns out that the impurity couples directly only to the fundamental harmonic, the other terms couple only indirectly through the first term and decouple in the limit $\Lambda \to 1$.

- 4 - Lanczos tridiagonalization: Wilson chain. The previous step ended up with the impurity coupled to a $p = 0$ term for each interval, in order to be able to solve it iteratively, it is tridiagonalized using the Lanczos algorithm. This results into a semi-infinite chain (the so called Wilson chain) in which the impurity couples on to its first site. The nearest neighbor couplings within the chain decays as $\Lambda^{-n/2}$ (for large n). This ensures a energy scale separation at each step.

- 5 - The renormalization group transformation A recursion relation is obtained: $H_{N+1} = \sqrt{\Lambda} H_N + \Lambda^{N/2} \sum_{\sigma} (t f^{\dagger}_{\sigma,N} f_{\sigma,N+1} + h.c.)$ that allows to define a renormalization group transformation $H_{N+1} = R(H_N)$.

- 6 - Iteration with truncation of the eigenvalues and eigenvectors. Because the Hilbert space grows exponentially one cannot keep up all states and energies while new sites are added, a truncation scheme is applied. The high energy states that are discarded do not affect the low energy states that are added. Each step corresponds to an energy scale associated to a given temperature.

4 Results: Scaling equations

Our quantum impurity problem consists of an interacting quantum impurity (QI) coupled to a metallic lead, as well as to a semiconducting contact (see Fig. 1). The effective density of states (DOS) seen by the quantum impurity, is also depicted in the left panel in Fig. 1, where it is clearly shown that there is a residual DOS around the Fermi energy, coming from the coupling of the QI to the metallic lead. The system is described by a Hamiltonian $H_{\rm SIAM} = H_{\rm imp} + H_{\rm S} + H_{\rm M} + H_{\rm Hyb}$, whose first term is given by

$$H_{\rm imp} = \sum_{\sigma} \varepsilon_d d^{\dagger}_{\sigma} d_{\sigma} + U n_{d\uparrow} n_{d\downarrow}, \tag{4.1}$$

where $d^{\dagger}_{\sigma}$ (d_{σ}) creates (annihilates) an electron with energy ε_d and spin $\sigma =\uparrow,\downarrow$ in the QI, $n_{d\sigma} = d^{\dagger}_{\sigma} d_{\sigma}$ is the QI occupancy, and U represents the Coulomb interaction. The leads are described by

$$H_{\rm S/M} = \sum_{\substack{\mathbf{k}\sigma \\ a={\rm S,M}}} \varepsilon_{a\mathbf{k}} c^{\dagger}_{a\mathbf{k}\sigma} c_{a\mathbf{k}\sigma}, \tag{4.2}$$

where $c^{\dagger}_{a\mathbf{k}\sigma}$ ($c_{a\mathbf{k}\sigma}$) creates (annihilates) an electron with momentum $\mathbf{k}$, energy $\varepsilon_{a\mathbf{k}}$ and spin σ in the metallic ($a = {\rm M}$) or in the semiconducting ($a = {\rm S}$) lead. Finally, the QI-leads hybridization is given by

$$H_{\rm Hyb} = \sum_{\substack{\mathbf{k}\sigma \\ a={\rm S,M}}} \left(V_{a\mathbf{k}} d^{\dagger}_{\sigma} c_{a\mathbf{k}\sigma} + {\rm H.c.} \right), \tag{4.3}$$

where $V_{a\mathbf{k}}$ represents the hybridization matrix element that couples the impurity either to the metallic ($a = {\rm M}$) or to the semiconducting ($a = {\rm S}$) lead. Here, we assume that the metallic lead is characterized by a flat DOS $\rho_M(\omega) = (1/2D)\Theta(D - |\omega|)$, where D is the half band width (Θ is the Heaviside step function), while the semiconducting-lead DOS (schematically shown in Fig. 1) is given by

$$\rho_S(\omega) = \rho_0 \frac{|\omega|}{\sqrt{\omega^2 - \Delta^2}} \Theta(|\omega| - \Delta)\Theta(D - |\omega|). \tag{4.4}$$

Here, 2Δ is the semiconducting gap and $\rho_0 = \frac{1}{2\sqrt{D^2-\Delta^2}}$ is a normalization factor [see [38]]. Assuming $V_{a\mathbf{k}} \equiv V_a$ to be $\mathbf{k}$-independent, for simplicity, the hybridization functions are defined as, $\Gamma_a(\omega) = \pi V_a^2 \rho_a(\omega)$ (for $a = S, M$).

The Kondo physics in our model, for $\Gamma_S = 0$, corresponds to the traditional SIAM, which has been extensively studied over the last decades. Experimentally, the Kondo physics for magnetic impurities adsorbed in metallic surfaces has been studied through low-bias transport spectroscopy using an STM tip weakly coupled to the impurity. In

our setup, the metallic lead serves not only to represent the STM tip, but also plays an important role in the NRG calculations, as it introduces a small, but finite, hybridization function at energies inside the semiconducting gap 2Δ (see Fig. 1).

In this work, we focus on the regime in which the QI is so weakly coupled to the metallic lead, in comparison to its coupling to the semiconducting lead, i.e., $[\Gamma_{\rm M} \ll \Gamma_S^{(0)} = \Gamma_S(D)]$, that any possible Kondo screening generated by conduction electrons in the metallic lead will occur at temperatures much lower than those associated to possible Kondo screening occurring through electrons in the semiconducting lead. For our analysis in what follows, it useful to define $\Gamma_0 = \Gamma_{\rm M} + \Gamma_S^{(0)} \approx \Gamma_S^{(0)}$, since $\Gamma_{\rm M} \ll \Gamma_S^{(0)}$. For the sake of completeness, in this chapter we present a preliminary analysis, using Anderson's poor man's scaling [58, 5], highlighting the interesting interplay between T_K and Δ.

Similar to what has already been done in Chapter 2, we can find an new effective Hamiltonian considering the impurity in the single occupation regime. Note now that all calculations of Chapter 2 were performed for an impurity coupled to a one lead only [see 'traditional' Anderson Model in (2.2)]. But it can be easily generalized to two or more leads by replacing the indexes and summation in $\mathbf{k}$ to indexes and summations in $a, \mathbf{k}$, where a represents the lead. Then the general Kondo Hamiltonian for the QI coupled to two or more independent leads can be written as

$$\begin{aligned} H_{\rm K} &= \sum_{a\mathbf{k}\sigma} \varepsilon_{a\mathbf{k}\sigma} c^\dagger_{a\mathbf{k}\sigma} c_{a\mathbf{k}\sigma} + \sum_{\mathbf{k}\mathbf{k}'} J_{a\mathbf{k}\mathbf{k}'} \Big[S^z \left(c^\dagger_{a\mathbf{k}\uparrow} c_{a\mathbf{k}'\uparrow} - c^\dagger_{a\mathbf{k}\downarrow} c_{a\mathbf{k}'\downarrow} \right) \\ &\quad + S^+ c^\dagger_{a\mathbf{k}\downarrow} c_{a\mathbf{k}'\uparrow} + S^- c^\dagger_{a\mathbf{k}\uparrow} c_{a\mathbf{k}'\downarrow} \Big] . \end{aligned} \tag{4.5}$$

where as already mentioned, our quantum impurity problem consists in a QD coupled to the metallic ($a = \mathrm{M}$) and the semiconducting ($a = \mathrm{S}$) lead. In addiction the coupling term can be written now as

$$J_a(D) \simeq |V_a|^2 \left(-\frac{1}{\varepsilon_d} + \frac{1}{\varepsilon_d + U} \right) . \tag{4.6}$$

Remember that here, the magnetic impurity is weekly coupled with the metal such that $J_{\rm S} \gg J_{\rm M}$. So, under these condition, this model is close to the "traditional" obtained by (2.19). Moreover, since $J_{\rm M} << J_{\rm S}$, the poor man's scaling analysis will break down before the J_M affect the renormalization flow. Therefore, we can use the scaling equation for the coupling J (that was obtained in the equation (3.5)), replacing J with $J_{\rm S}$

$$\frac{dJ_{\rm S}}{d\ln\Lambda} = -2\rho(\Lambda) {J_{\rm S}}^2, \tag{4.7}$$

where $J_{\rm S}(D)$ can be obtained by (4.6).

So in this part, we will study the magnetic impurity coupled to only a semiconductor band with gap finite gap 2Δ between conduction and valence band. The density of states has the form (4.4), but the same analyzes can be done for any type of conduction band, changing only the complexity of the approach.

Replacing the form of density of states for this semiconductor band (4.4) in the β-equation (4.7) and integrating in the range $\Lambda^* \leq \Lambda \leq D$, we obtain

$$-\frac{1}{J_S(\Lambda^*)} + \frac{1}{J_S(D)} = -2\rho_0 \int_D^{\Lambda^*} d\Lambda \frac{\Theta(\Lambda - \Delta)}{\sqrt{\Lambda^2 - \Delta^2}}. \tag{4.8}$$

For this system there are no electrons in conduction band above the Fermi level if temperature is smaller than the gap $T < \Delta$. Hence, it is expected that there is no strong coupling limit if T_K is less than the gap. With this in mind, integrating the equation (4.8) for $\Lambda^* \leq \Delta$ renders

$$-\frac{1}{J_S(\Lambda^*)} + \frac{1}{J_S(D)} = -2\rho_0 \int_D^{\Delta} d\Lambda \frac{1}{\sqrt{\Lambda^2 - \Delta^2}} = K(\Delta, D), \tag{4.9}$$

where $K(\Delta, D)$ is a constant just as $J_S(D)$. So $\frac{1}{J_S(\Lambda^*)}$ must be in general case a non zero constant. Then, there is no strong coupling limit in this case.

However, if $\Lambda^* > \Delta$ we can find a regime with temperature between the Δ and T_K so that the Kondo effect sets down (unstable strong coupling fixed point). We can investigate this with the equation (4.8) by imposing the strong coupling in Λ^* by setting $1/J_S(\Lambda^*)$ to zero in Eq. (4.9), obtaining

$$\frac{1}{J_S(D)} = -2\rho_0 \int_D^{\Lambda^*} d\Lambda \frac{1}{\sqrt{\Lambda^2 - \Delta^2}} = -2\rho_0 \ln \left[\frac{\Lambda^* + \sqrt{\Lambda^{*2} - \Delta^2}}{D + \sqrt{D^2 - \Delta^2}} \right]. \tag{4.10}$$

Upon manipulating the equation (4.10) to isolate the Λ^*, finally, we can estimate the Kondo temperature for this semiconductor band as

$$T_K \sim \Lambda^* = \frac{1}{2} \left[\left(D_0 + \sqrt{D_0^2 - \Delta^2} \right) e^{-\aleph_1} + \frac{\Delta^2}{D_0 + \sqrt{D_0^2 - \Delta^2}} e^{\aleph_1} \right]. \tag{4.11}$$

Here the exponent $\aleph_1$ is given by

$$\aleph_1 = \frac{1}{2\rho_0 J_S(D)}. \tag{4.12}$$

We can clearly see that in the limit where the gap goes to zero, the density of state for this system tends to behave like a flat band and the corresponding expression for T_K obtained as well (3.6).

As mentioned before, Λ^* needs be in range $\Delta < \Lambda^* \leq D_0$ to Kondo regime occur. Using this in the equation (4.10) we find a range for the values of $J_S(D) > J_C$ so that the strong coupling limit can happen with

$$J_C = \left[2\rho_0 \ln \left(\frac{D_0 + \sqrt{D_0^2 - \Delta^2}}{\Delta} \right) \right]^{-1}. \tag{4.13}$$

The $J_S(D) = J_C$ is the minimum coupling for which the Kondo effect can occur. $J_S(D)$ can be found by equation (4.6) in terms of the V_S, ε_{dS} and U_S.

Note that it has already been discussed, but we need to pay attention to the fact that the ground state for this problem is not the Kondo singlet. The Kondo effect can occur only for energies between the gap Δ and T_K. This result is different from what we found for the 'traditional' Kondo problem, where the system continues in the Kondo singlet all the way to $T \to 0$. Then, in our problem the Kondo singlet is a transition state, called unstable strong coupling fixed point. For energy below the gap, the impurity is expected to be decoupled to the conduction band in single occupancy state.

Although the results obtained are interesting, the Kondo Hamiltonian is not able to explain the FO fixed point regime, since we obtained this model by imposing that the system is in LM fixed point. So, for this type of analysis it is more appropriate to use the scaling equations $\tilde{U}$, $\tilde{\varepsilon}_d$ and $\tilde{V}$ obtained by poor man's scaling for the Anderson model. In the particle-hole symmetry regime, $\tilde{\varepsilon_d} = -\tilde{U}/2$, and for conduction band hybridization function with even symmetry $\Gamma(\Lambda) = \Gamma(-\Lambda)$, we can unify the equations (3.34) and (3.33) in a single equation

$$\frac{d\tilde{U}}{d\Lambda} = \frac{16\Gamma(\Lambda)}{\pi} \frac{\tilde{U}}{4\Lambda^2 - \tilde{U}^2}. \tag{4.14}$$

Following the idea already discussed above, we can generalize this equation to two or more leads by changing the hybridization function $\Gamma(\Lambda)$ by $\sum_a \Gamma_a(\Lambda)$, where a represents the lead under consideration.

Despite its apparent simplicity, we have not been able to find an analytical solution to equation (4.14). We provide instead a numerical one, shown in Fig. 7 (red curve). The red curve shows the solution $\tilde{U}(\Lambda)$ for the equation (4.14). Given the low-order perturbative approach in derivation of equation (4.14), it cannot provide quantitative accurate results, as it expected to be rigorously valid for $\Lambda \gg \tilde{U}, \tilde{\Gamma}$ [64]. In particular, it is known that Eq. (4.14) is unable to describe correctly the physical regimes if $\tilde{\Gamma} > \Lambda > \tilde{U}/2$ [32], however it shows that $\tilde{U}$ rapidly decreases with Λ.

It is well-known that in the Anderson Model at temperature $T > U$ the electrons in the system are in a FO fixed point (were the QD states $|\tilde{0}\rangle$, $|\tilde{1}_\uparrow\rangle$, $|\tilde{1}_\downarrow\rangle$ and $|\tilde{2}\rangle$ are equally likely) since the electrons have enough energy to overcome the Coulomb repulsion. This occurs in the plot of the Figure 7 when $\Lambda > \tilde{U}, \tilde{\Gamma}$. As the temperature decreases, eventually, $T < U$ and now the electrons in QI states feel the Coulomb repulsion and the state of one electron occupation ($|\tilde{1}_\uparrow\rangle$ or $|\tilde{1}_\downarrow\rangle$) are more likely. In other words, the QI are in a LM fixed point. According to Cheng *et al.* [Ref. [32]], this occurs where $\tilde{U} > \Lambda, \tilde{\Gamma}$. Also, if $\tilde{\Gamma} > \Lambda > \tilde{U}$, then the system can be in a mixed-valence state or in a strong coupling regime. Using the Eq. (4.11), we can estimate the Kondo temperature $T_K \sim 10^{-3}$. At that point, the system QD and conduction band form a characteristic singlet (SC fixed point) where the effective coupling $J \to \infty$. Note that in equation (2.21), the effective coupling $\tilde{J}$

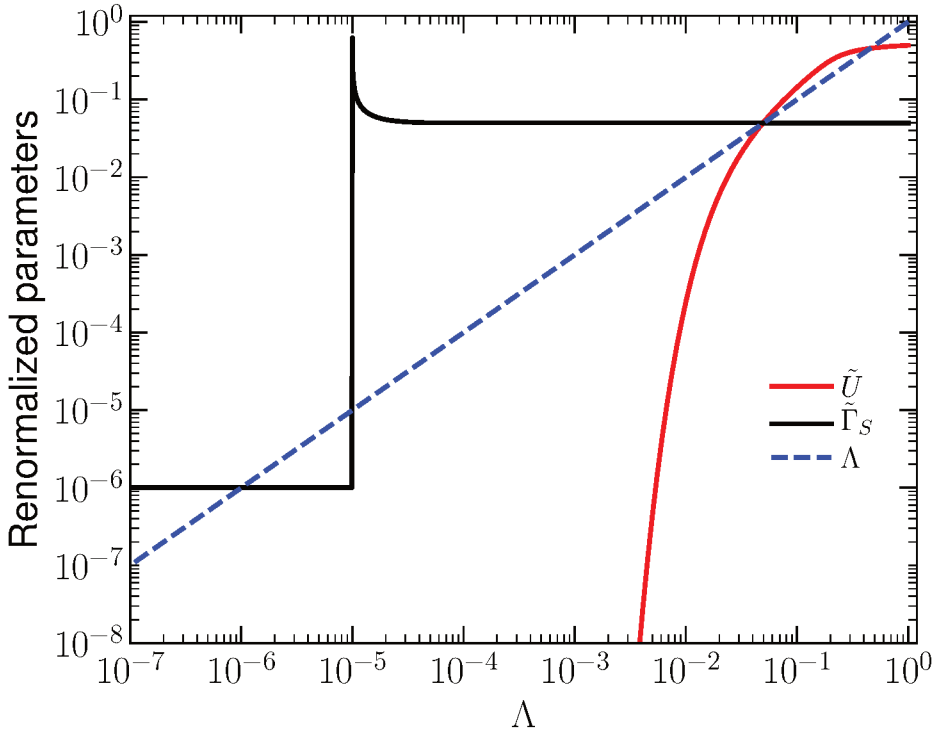

Figure 7 – Renormalized parameters of the SIAM: $\tilde{U}$ (red) and Γ (black) obtained by applying Anderson's poor man's scaling to the SIAM. Bare parameter values used were $U = 0.5$, $\Delta = 10^{-5}$, $\Gamma_M = 10^{-6}$, and $\Gamma_S = 0.05$. Blue dashed line shows Λ for a better comparison to the other curves. The point where Λ becomes larger than $\tilde{\Gamma}$ and $\tilde{U}$ indicates that the system reenters the mixed valence regime.

can be rewritten in terms of the effective parameters as

$$\tilde{J} \simeq |\tilde{V}|^2 \left(-\frac{1}{\tilde{\varepsilon}_d} + \frac{1}{\tilde{\varepsilon}_d + \tilde{U}} \right). \tag{4.15}$$

If $\tilde{U} \to 0$ the effective coupling $\tilde{J} \to \infty$, which is consistent with the results of Fig. 7. Using only the above discussion, we can conclude that the system is in a Kondo singlet, at least for the temperatures within range between T_K and Δ ($T_K > \Lambda > \Delta$). Now, let us look closely at the energy range $10^{-5} > \Lambda > 10^{-6}$. In this range, $\Lambda > \tilde{\Gamma} > \tilde{U}$. The reader my ask the question whether, in this situation, the system not behave like FO fixed point? Unfortunately, the PMS analysis is not able to answer this question, since the perturbation technique fails to describe the system in the SC fixed point. We, therefore, need a more powerful tool that solves the problem in a non-perturbations way. The ideal technique is the NRG, already introduced in the previous chapter.

5 Results: Numerical Renormalization Group Approach

The renormalization analysis presented so far was very useful to grasp a general qualitative idea of the interplay between the various parameters of our system model. For a deeper quantitative understanding of the underlying physics, in this chapter we use the NRG method, introduced in chapter 3. All NRG calculations was performed using the NRG Ljubljana code [see [62] and [63]]. The NRG can numerically solve the Kondo problem using the Anderson model or the Kondo model itself and find thermodynamic properties at any temperature scale. We chose to use the Anderson model to find these properties since we want to understand the physics of the system from the energy scales of the order of the conduction band all the way deeper below the gap. To obtain the results within the NRG we set the bandwidth of both semiconductor and metallic contact as $D = 1$ as our energy unit. Moreover, for simplicity we set $K_B = \hbar = 1$ so temperature is also given in unity of energy D.

5.1 Thermodynamic properties for $\Gamma_{\mathrm{M}} \approx 0$

Here we want to discuss the case where the impurity is coupled only with the semiconductor-lead. To do this, in this section, we set $U = 0.5$, $\varepsilon_d = -0.25$ and $\Gamma_{\mathrm{M}} = 10^{-10}$. We also want to compare the results obtained by the poor man's scaling in the Kondo model and discuss how it helps understanding the NRG results. Having a clear picture of the physics discussed in this section is very important to understand the main results of this work which will be presented in the next section.

To understand the various fixed point of the system within the NRG calculations, it is very useful to analyses the impurity entropy S_{imp} vs temperature T. The contributions of the impurity to thermodynamic properties, such as S_{imp}, are defined by the difference between this properties with the impurity and without it. In statistical mechanics we can prove that the entropy at zero temperature is $\ln(m)$ (in units of k_B) where m is the degeneracy. If the state is a singlet the entropy goes to zero, this is the case of the Kondo effect where the impurity forms a singlet with the electrons of the conduction band. In the local moment regime (one-electron with spin up or down) this state represents a doublet and the entropy goes to $\ln 2$. At high temperatures the electrons in quantum impurity are in a Valence mixed regime where the states $|\tilde{0}\rangle$, $|\tilde{1}_{\uparrow}\rangle$, $|\tilde{1}_{\downarrow}\rangle$ and $|\tilde{2}\rangle$ are equally likely, then the entropy goes to $\ln 4$.

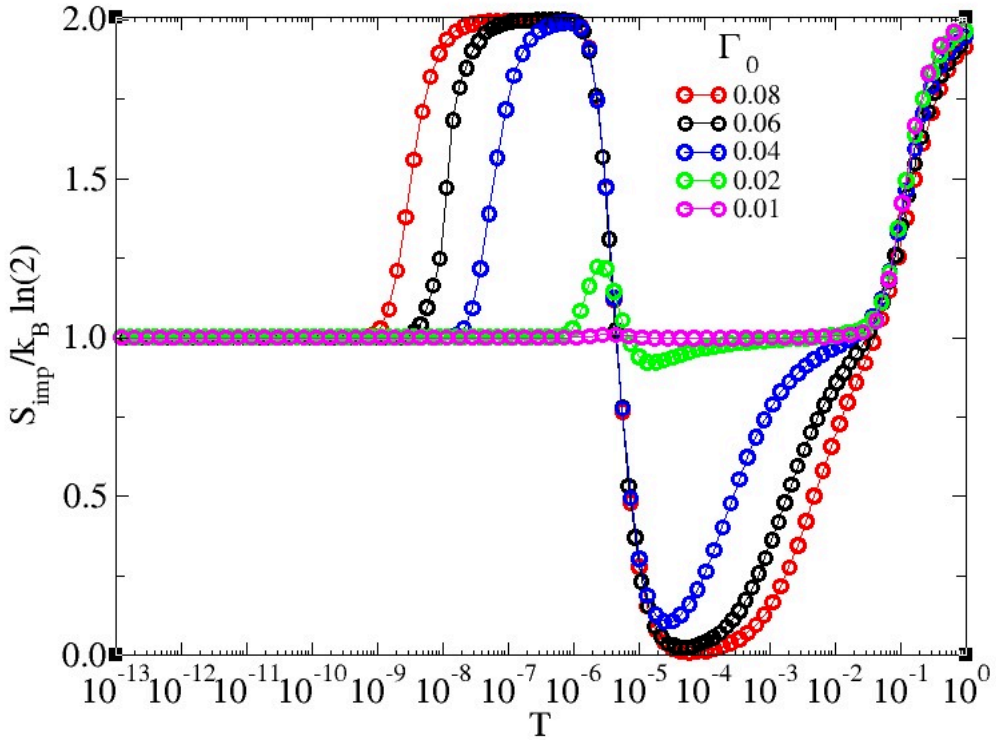

Figure 8 – Impurity entropy behavior for $U = 0.5$, $\varepsilon_d = -0.25$, $\Delta = 10^{-5}$ and different values for Γ_0. The critical coupling for this case is $\Gamma_0 = 0.028$ by Wilson's criterion. In the graph we note a big behavior change between Γ_0 values 0.02 and 0.04.

In Fig. 8 we show the NRG result for the impurity entropy, as function of temperature, for different values of Γ_0. Let us start the discussions with $\Gamma_0 = 0.04$ (blue circles) at high temperatures $T > U = 0.5$. This is the Valence mixed regime, in which the electrons have energy enough to overcome the Coulomb repulsion, then the states $|\tilde{0}\rangle$, $|\tilde{1}_\uparrow\rangle$, $|\tilde{1}_\downarrow\rangle$ and $|\tilde{2}\rangle$ are equally probable. However, for temperatures $0.5 > T \gtrsim 10^{-3}$ the electrons in quantum impurity sense the Coulomb repulsion, then the states $|\tilde{1}_\uparrow\rangle$ and $|\tilde{1}_\downarrow\rangle$ are now more likely and the entropy goes to $\ln 2$. In this case, the quantum impurity has a resultant local moment, in other words, this correspond to the LM regime. As the temperature further decreases the conduction electrons start "feeling" the presence of the impurity. If the coupling between the electrons in impurity and the electrons of the conducting band is strong enough ($\Gamma_0 \geq \Gamma_C$), the impurity and conduction band system becomes a singlet known as the Kondo singlet for temperature below the characteristic temperature known as $T_K \sim 10^{-3}$ (for $\Gamma_0 = 0.04$, blue curve in the Fig. 8). Where Γ_C are the critical hybridization and can be related to J_C, in the p-h symmetry, by $J_C = \frac{8}{\pi}\frac{\Gamma_C}{U}$. For the parameters used the $\Gamma_C = 0.28$ and it will be discussed in more detail below. We can observe in Fig. 8, that if $\Gamma_0 \geq 0.28$ (red, black and blue curves) the impurity entropy falls significantly indicating that the onset of the Kondo singlet state. If $\Gamma_0 \ll 0.28$ (pink and green curves) the electrons in the conduction are weakly coupled from the impurity to any temperature, but if $\Gamma_0 \gg 0.28$ the behavior at the gap is the exactly what was discussed above.

Continuing the discussions of Fig. 8, we can estimate the $T_K \sim 10^{-7}$ for $\Gamma_0 = 0.02$ (green curve) by Eq. 4.11. But, as previous discussed in chapter 4, if $T_K < \Delta$ has no Kondo screening. Below the gap, there are no electrons in the conduction band, then if temperatures is less than Δ, the system have a abrupt change in the "number" of conduction electrons. Thus, the electrons in quantum impurity are decoupled to the conduction band in a doublet state ($|\tilde{1}_\uparrow\rangle$ and $|\tilde{1}_\downarrow\rangle$). In this case, for $\Gamma_0 = 0.04$ (blue curve) the singlet are destroyed and the system returns to the LM fixed point and the entropy always goes to $\ln 2$ (we can see this at temperatures $T < 10^{-8}$). However, for temperatures in the range $10^{-8} < T < 10^{-5}$, that's not exactly what happens. Note that in this range, something like $T > U$ occurs, a second Valence mixed regime (a second FO regime). Also in the Figure 8 we note the FO and LM regimes appear to be repeated below the gap for many curves (red, black and blue curves). So, a question arises: Is Anderson's model repeating itself with the renormalized parameters $\tilde{U}$, $\tilde{V}$ and $\tilde{\varepsilon}_d$? The answer is yes, and we call it reentrant SIAM.

Even though our poor man's scaling in Anderson Model approach does not provide a quantitative reliable result for $\tilde{U}$, it suggest us that the coulomb repulsion appearing in the reentrant SIAM should be very small, and and this is consistent to what is seen in Fig. 7. The reentering of the system into the mixed valence regime can be understood by comparing $\tilde{\Gamma} = \Gamma(\Lambda)$ (black line) with Λ. Note that for for $\Lambda < \Delta$, the effective hybridization function suddenly drops to Γ_M which is smaller the Λ. In the RG sense, Λ is directly related to the temperature T of the NRG calculation. Having this in mind, we expect the system to reenter the FO regime for $\Lambda \approx \Delta = 10^{-5}$. These reasoning's explain at least qualitatively why the system returns to the FO fixed point shown in Figure 8 evolves as a second stage effective Anderson model, exhibiting all the expected fixed points. Since this is a perturbative renormalization analysis, it is not expected to provide an accurate result where the system enters into a Kondo regime, nevertheless it provides a very interesting picture of the underlying renormalization flow.

Remember that, for technical reasons, the hybridization function cannot be zero within the gap, so we need to put a very small but finite value. After all this discussion one can be led to think, if we have below the gap a second SIAM (reentrant SIAM) with renormalized parameters $\tilde{U}$, $\tilde{V}$ and $\tilde{\varepsilon}_d$. Maybe at temperature $T \ll \Delta$ we also have a second Kondo regimen (with $T_{K2} \ll T_{K1}$) if the hybridization function Γ_M, is small, but finite into the gap. The answer is again yes! We will discuss this regime in the next section.

As mentioned in the Introduction, we know that there is an artifact of the poor man's scaling approach, since, at half filling, as shown through NRG and confirmed by other methods, there is no SC fixed point for any finite gap Δ in the semiconductor spectra. In the following, we will compare the critical coupling given by equation (4.13) with the corresponding numerical results obtained from NRG calculations for the appropriate

Anderson model. To do so, it is convenient to express J_C in terms of the Anderson model parameters. Defining $\Gamma_S^{(0)} = \pi V_S^2 \rho_0$, we can write $J_S^{(0)} = 4V_S^2/U = 4\Gamma_S^{(0)}/(\pi\rho_0 U)$, at the particle-hole symmetric point. Thus, equation (4.13) can be rewritten as

$$\Gamma_c = \frac{\pi U}{8}\left[\ln\left(\frac{D+\sqrt{D^2-\Delta^2}}{\Delta}\right)\right]^{-1}. \tag{5.1}$$

To compare the results for the semiconductor with gap obtained by Poor man's scaling with different values of Δ, for each value of Δ we search for a critical value Γ_C, the $\Gamma^{(0)}$ below which the Kondo effect ceases to occur.

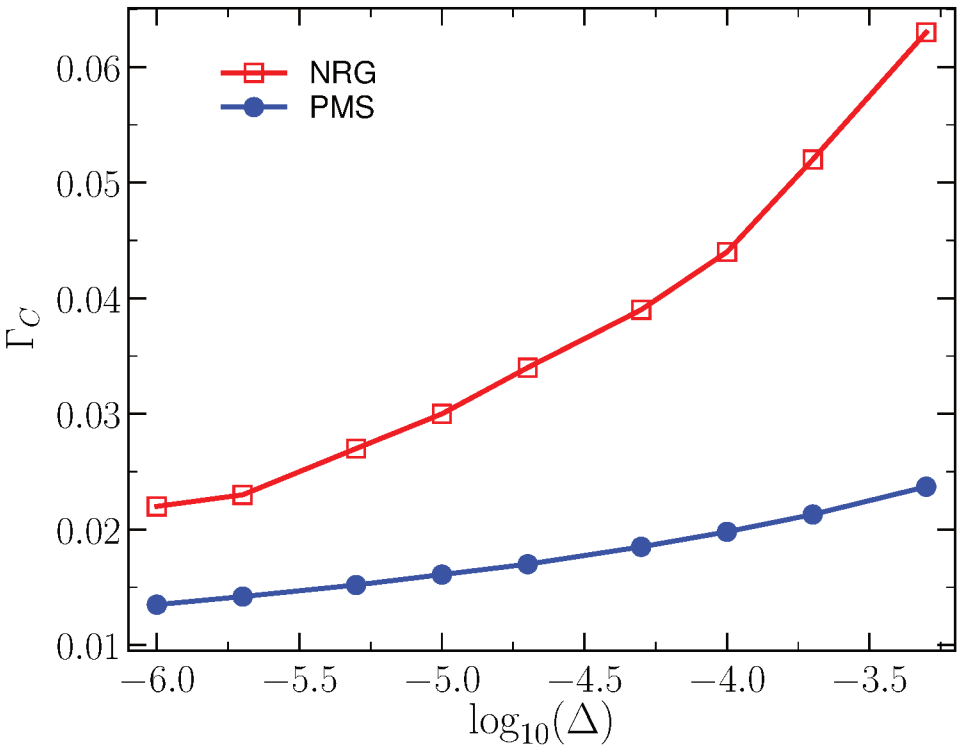

Figure 9 – Γ_C obtained by poor man's scaling [(red) squares] and by NRG [(blue) circles] for different values of Δ. The bare parameter values were $U = 0.5$ and $\varepsilon_d = -0.25$. Note that the qualitative behavior between the curves is similar, however when comparing quantitative we observe that the NGR curve (red squares) increases more fast then the PMS (blue circles).

In Figure 9 we plot Γ_C vs Δ for $U = 0.5$ (blue circles) as obtained through the expression in (5.1) and compare it with the critical Γ_C obtained by NRG (red squares). To determine whether there is Kondo screening or not in the NRG calculations we monitor the impurity magnetic moment $k_B T\chi_{\rm imp}(T)$ for decreasing temperature. Following Wilson's criterion [5], we say that the Kondo screening takes place only if magnetic moment becomes smaller than 0.07 as the system is cooled down. Thus, Γ_C is the smallest value of $\Gamma^{(0)}$, as obtained through NRG (red dots in Figure 9), for which this condition is still satisfied. The resulting Γ_C (as a function of Δ) obtained through NRG is systematically larger than the obtained by poor man's scaling (equation (9)). We note that there is a qualitative

agreement between the PMS and the NRG results, showing that Γ_C increases with Δ. This means that, as intuitively expected, a larger Δ requires stronger hybridization between the impurity and the conduction electrons for the Kondo screening to take place. Last, but not least, taking into account that, as shown above, there is no SC fixed point for $\Lambda < \Delta$, the NRG results in Figure 9 (red dots) do not describe the ground state of the $V_M = 0$ Hamiltonian, but rather what we may call a finite-temperature-Kondo (see below) associated to an unstable SC fixed point. As described in the Introduction, the ground state of the $V_M = 0$ Hamiltonian corresponds to a doublet LM fixed point [53, 54].

5.2 Thermodynamic properties for $\Gamma_S \gg \Gamma_M$: reentrant SIAM

Here we discuss effect of small, but finite, Γ_M. In which case, the system will be described by a reentrant renormalized Anderson Hamiltonian (reentrant SIAM) and the conditions under which the second Kondo regime is possible. In particular, we are interested in studying what happens to the system for temperatures below T_{K1}, where, again, $T_{K1} > \Delta$ is the Kondo temperature for $V_M = 0$ (T_K for a unstable SC regime). To do this, are fixed $U = 0.5$, $\Gamma_S(D) + \Gamma_M = \Gamma_0 = 0.05$ and $\Delta = 10^{-5}$, in which case the first Kondo screening is possible. Our results now rely just on NRG calculations, as the PMS breaks down before $\Lambda < \Delta$. We will see how the intriguing effective Anderson Hamiltonian is observed as the temperature goes to zero. This assertion will become clear after we analyze the impurity thermodynamic properties.

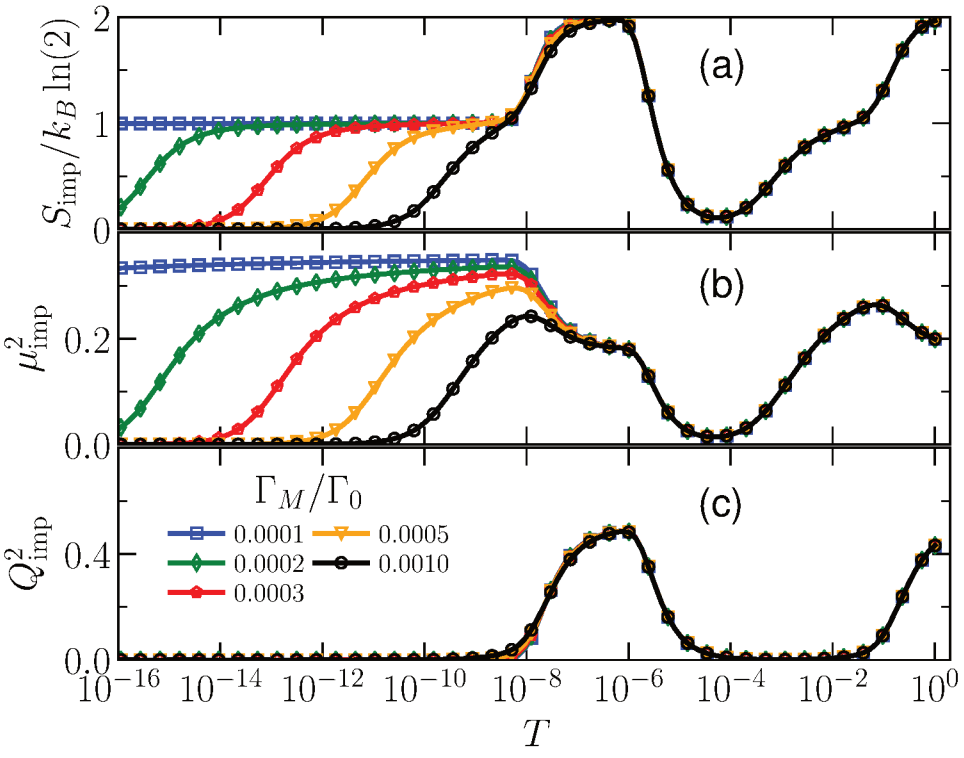

Figure 10 – Impurity contribution to (a) Entropy S_{imp}, (b) magnetic moment μ_{imp}, and (c) charge fluctuation ΔQ^2, as a function of temperature for $0.0001\Gamma_0 < \Gamma_M < 0.001\Gamma_0$. Note the appearance of a second SC fixed point (for all $\Gamma_M \geq 0.0002\Gamma_0$) at lower temperatures, which can be identified by an increase in charge fluctuation at around $T \approx 10^{-5}$ [panel (c)], followed by an LM regime, followed by an impurity-band singlet formation [panel (b)] at the second SC point, with lowering onset temperature, as Γ_M decreases. See details in the text.

In the Figure 10 we show the impurity contribution to the entropy, $S_{\rm imp}$ [Fig. [10(a)], magnetic moment, $\mu_{\rm imp}$ [10(b)], as well as the charge fluctuations, ΔQ^2 [10(c)], as a function of temperature for various values of Γ_M. We first note that, for temperatures above the gap $T > \Delta$, we observe the traditional SIAM behavior, in which the system crosses over from the FO to the LM to a SC fixed point, as the temperature decreases. As previously discussed, these three fixed points are marked, respectively, by entropy values $S_{\rm imp}/k_B \sim \ln 4$, $\sim \ln 2$, and 0, as seen in Figure 10(a). This is accompanied by an enhancement of the magnetic moment $\mu_{\rm imp}$, at the LM fixed point, followed by its complete suppression in the SC fixed point, as shown in Fig. 10(b). Finally, notice also the strong suppression of the impurity charge fluctuations ΔQ^2 (at the LM and SC points) [Figure 10(c)]. Interestingly, all these features are independent of the Γ_M value. This can be easily concluded from the superposition of all the curves in all panels in Figure 10 in the temperature interval $10^0 > T > 10^{-5}$. This behavior is associated to the fact that in all calculations Γ_0 are fixed, thus the hybridization function is always the same above the gap.

It is well-known that the thermodynamic properties presented above are characteristic of the SIAM [5]. However, for a *traditional* SIAM, the values of the thermodynamic quantities, for $T \ll T_K$, i.e., well into the SC regime, remain unchanged down to $T \to 0$, as the system would have already reached the stable SC fixed point and would stay there. Remarkably, in the present case, when T approaches $\Delta = 10^{-5}$ (from above), the system deviates from this standard behavior, as it can be easily seen in Fig. 10, since all thermodynamic properties have additional structures for $T < \Delta$. Indeed, when $T \to \Delta$, the system flows to a *second* free orbital (SFO) fixed point, marked by an increase of $S_{\rm imp}$, $\mu_{\rm imp}$, and ΔQ^2, to values that go back to their high temperature ($T = D$) values. Further decrease of T shows that the system crosses over fixed points that are very similar to the ones crossed in the temperature interval $10^0 > T \gtrsim 10^{-5}$. The similarity between the low and high temperature fixed points indicates that, for $T < \Delta$, the system seems to be governed by an effective SIAM with renormalized parameters and a much lower Kondo temperature. Note that the extent of the plateaus in the entropy (at $k_B \ln 2$) and in the magnetic moment (at $\approx 1/4$) depend strongly on Γ_M, showing that the second stage Kondo temperature, denoted as T_{K2}, depends strongly on Γ_M. Thus, all thermodynamic quantities (S_{imp}, $\mu_{\rm imp}$, and $\Delta Q^2_{\rm imp}$) exhibit behavior compatible with the NRG flow of a second stage effective SIAM.

The reentrant SIAM below the gap, can be understood as the same SIAM model but with renormalized effective parameter $\tilde{U}$, $\tilde{\varepsilon}_d = -\tilde{U}/2$, $\tilde{\Gamma}_0$ and $\tilde{\Gamma}_M$. Through the PMS in SIAM we have evidence that the hybridization functions (Γ_M and Γ_S) are not affected significantly in the scaling procedure. Another information given by PMS is the fall of the effective Coulomb repulsion as the temperature decreases, despite the PMS not providing quantitative information below T_{K1}, we can believe in the qualitative discussion about these results. However by Figure 10, the second FO fixed point occur in temperature range

$10^{-5} \gtrsim T \gtrsim 10^{-8}$. It's expected that occur where $\Delta > T > \tilde{U}$, then we can conclude that the effective Coulomb repulsion below the gap is on the order of magnitude $\tilde{U} \approx 10^{-8}$ and has little or any dependency with Γ_M. For temperatures $T < 10^{-8}$ the system goes to the second LM fixed point, until for a finite Γ_M the system goes to a second (stable) SC fixed point for temperatures $T < T_{K2}$.

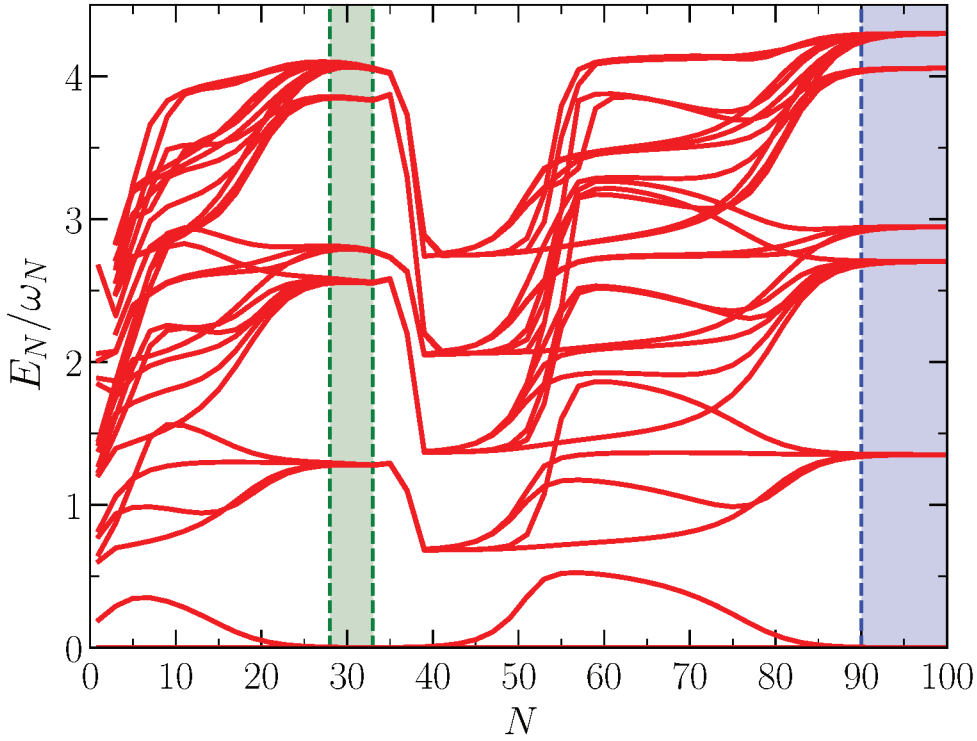

Figure 11 – Energy spectrum vs NRG iteration step N (odd). Note the fixed points in the traditional Anderson model seen in the iterations ranging from $N = 0$ to $N \approx 35$, which are repeated for the higher iterations step number ($N > 35$), showing the reentrance of the Anderson model behavior at low energies. The model parameters used here are $\Gamma_0 = 0.05$, $\Gamma_M = 5 \times 10^{-4}$.

This unusual interesting behavior can be clearly captured from the energy flow diagram obtained from NRG, as we show in Figure 11, for the energy spectrum as function of NRG iteration step N (odd). The *traditional* SIAM fixed points are observed in the range of iterations from $N = 0$ to $N \approx 35$, while the second stage SIAM fixed points are repeated for the higher iterations step number ($N > 35$). For the sake of clarity, we have shade in green the (unstable) SC fixed point and in blue shade the second (stable) SC fixed point.

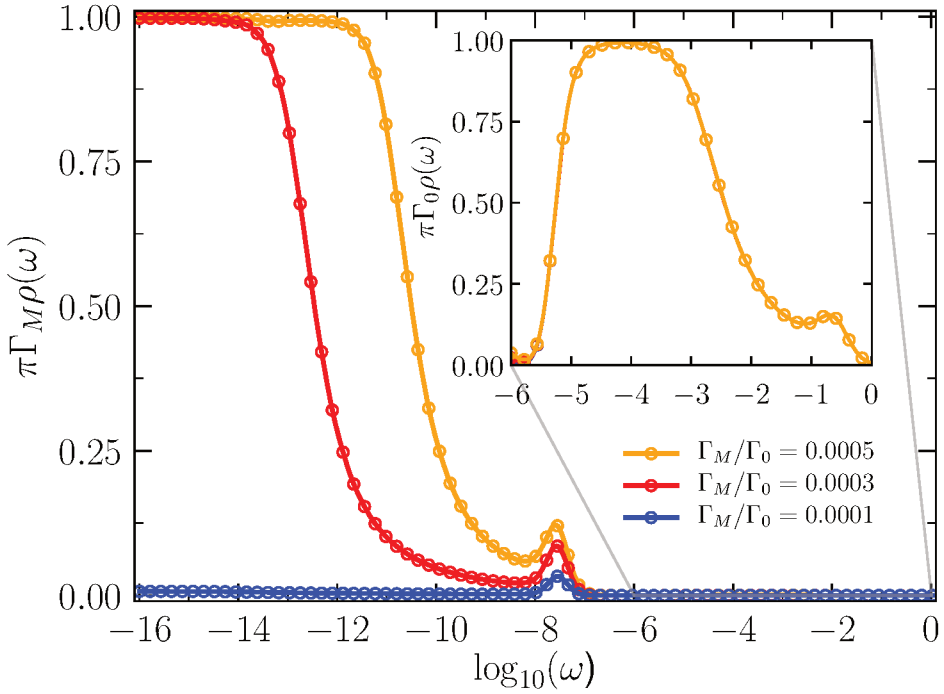

Figure 12 – Local density of states vs energy for $\Gamma_0 = 0.05$ and various values of Γ_M. The inset shows a zoom-in of the region of the first Kondo regime. The vertical axis of the main panel and the inset are multiplied by $\pi\Gamma_M$ and $\pi\Gamma_0$, respectively, so as to shown that the Kondo regimes obey their expected Friedel sum rule. In the horizontal axis we show $\log_{10}(\omega)$ for clarity and we restricted to positive values of ω. The curves exhibit particle-hole symmetry, $\rho(-\omega) = \rho(\omega)$, so the results for negative energies are not shown, for simplicity.

To continue the discussions about the reentrant SIAM, we now need a way to measure U_{eff} at NRG. One way to do that and also get further insights on the two Kondo fixed points can be seen from the local density of state LDOS

$$\rho(\omega) = -\frac{1}{\pi}\langle\langle d_\sigma; d_\sigma^\dagger\rangle\rangle_\omega \tag{5.2}$$

where $\langle\langle d_\sigma; d_\sigma^\dagger\rangle\rangle_\omega$ is the retarded local green's function in the energy domain in the Zubarev's notation [65]. Here, $\rho(\omega)$ is calculated within the NRG calculation [66]. Figure 12 shows $\pi\Gamma_M\rho(\omega)$ (in the main panel) and $\pi\Gamma_0\rho(\omega)$ (in the inset) vs $\log_{10}\omega$ for various values of Γ_M. Note in the main panel of Figure 12 that for $\Gamma_M = 10^{-4}\Gamma_0$ (blue curve) we see no Kondo peak for ω as small as 10^{-16}. However for $\Gamma_M = 3\times10^{-4}\Gamma_0$ and $\Gamma_M = 5\times10^{-4}\Gamma_0$ (red and orange curves, respectively), the Kondo peaks pronounce fulfilling nicely the Friedel sum rule. The small peaks observed slightly above $\omega = 3\times10^{-8}$ corresponds to the Hubbard peak associated to the renormalized coulomb repulsion U_{eff} of the effective SIAM. Likewise, the inset shows a zoom of the region of $\omega \in [10^{-6}, 1]$, note that curves collapse onto each other. The highest peak corresponds to the first Kondo effect, while the small peak above $\omega = 10^{-1}$ correspond to the Hubbard peak, associated to U. Identifying U_{eff} here is very useful for a fully understanding of the results of Figure 10. It is clear

that as the temperature decreases, the system enters as second FO fixed point at $T \sim \Delta$, where $\Gamma(\omega)$ drops to Γ_M, in which case we have $T > \Gamma, U_{\text{eff}}$. The system enters the second LM fixed point when $T \lesssim U_{\text{eff}} \approx 6 \times 10^{-8}$. Finally, when T goes below the second Kondo temperature (T_{K2}) the system reach the stable SC fixed point. The existence of this small U_{eff} can be understood within the poor man scaling analysis in the Anderson model, discussed in the previous section. Note, however, that the scaling calculations for the parameters in Anderson model by PMS are continuous, while the results found through LDOS in NRG are discrete (only one U_{eff} peak for example). Similar analyzes were performed also by Jefferson [67] and Haldane [59] for metallic conduction bands and latter on extended to a more general problem by Cheng Ref. [64] and [32]. Although these analysis are limited by their perturbative character, they suggest that the renormalized coulomb repulsion indeed decreases along the RG flow.

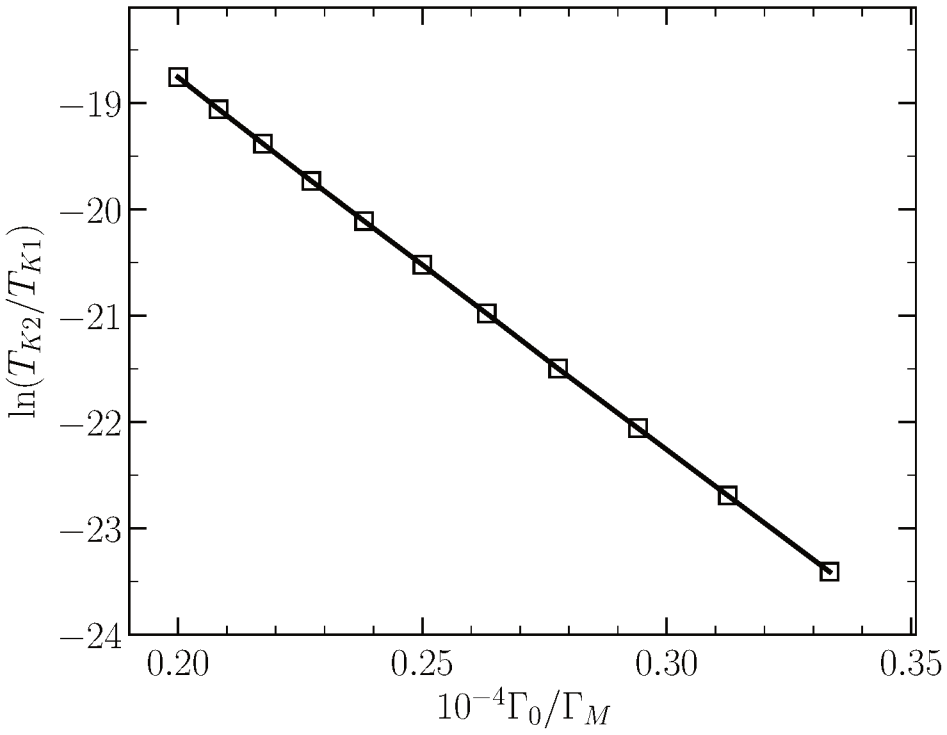

Figure 13 – $\ln(T_{K2}/T_{K1})$ vs Γ_0/Γ_M for $\Gamma_S = 0.05$. From the linear behavior of the curve e can extract an expression $T_{K2} = A_0 e^{-A_1/\Gamma_M}$.

The value of ω where the red and yellow curves of the main panel of Figure 12 cross 1/2 can be identified as the Kondo temperature of the reentrant Kondo screening, T_{K2}. For a better visualization of the dependence of T_{K2} on Γ_M, in Figure 13 we show $\log(T_{K2}/T_{K1})$ vs Γ_0/Γ_M for a fixed $\Gamma_0 = 0.05$. The linear behavior of the curve suggest an expression for T_{K2} as $T_{K2} = A_0 e^{-A_1/\Gamma_M}$. While precise values of A_0 A_1 are not important here, the exponential behavior is remarkable as it is similar to Haldane expression for $T_K \sim e^{-\pi U/8\Gamma}$ for the particle-hole symmetric point [5]. Here the parameters A_0 and A_1 carry the intricate information from the renormalized effective Anderson model.

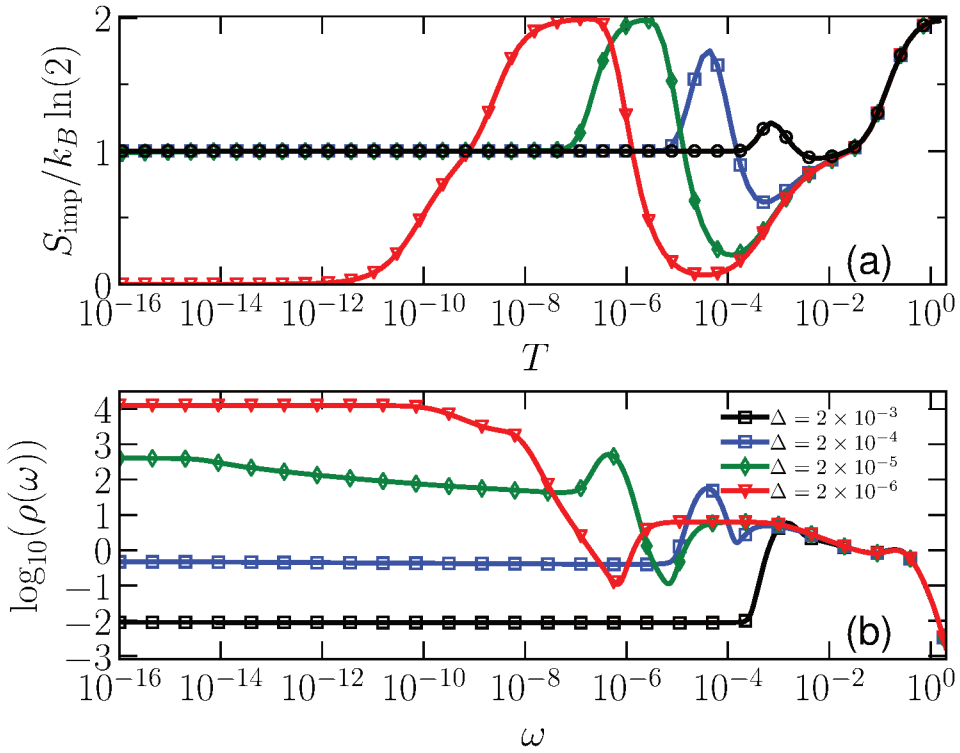

Figure 14 – (a) Entropy vs T and (b) $\log_{10}[\rho(\omega)]$ vs energy for $\Gamma_S = 0.05$, $\Gamma_M = 5 \times 10^{-4}$ and various values of Δ. We have chosen to show $\log_{10}[\rho(\omega)]$ to visualize all the peaks, as their height differ by several order of magnitude. Note that for $\Delta = 2 \times 10^{-6}$ (red curve), the entropy vanishes as $\omega \to 0$ while both Kondo peaks are fully developed. However, as Δ increases, the first Kondo fixed point is squeezed from below, the entropy goes to $k_B \ln(2)$ as $\omega \to 0$ and the second Kondo peak is progressively suppressed.

After the form of Haldane expression works well for T_{K2}xΓ_M, we also need to test the dependence of T_{K2} with U_{eff}. Before we do this, we need to find a way to change the value of U_{eff}. In Figure. 14 we show how these Kondo screening and the U_{eff} change as Δ changes. Figure 14(a) and Figure 14(b) show the entropy and the LDOS, respectively. Note that for $\Delta = 2 \times 10^{-6}$ (red curve) the S_{imp} is strongly suppressed for T in the region $10^{-5} - 10^{-4}$ and vanishes as $T \to 0$, showing clearly the existence of the two Kondo screening regimes. The LDOS, consistently, exhibits the two Kondo peaks with their respective heights $1/(\pi\Gamma_0)$ and $1/(\pi\Gamma_M)$, respectively, in the first and in the second Kondo regimes. However, for the

other values of Δ shown in Figure 14 we note that the first Kondo regime is progressively destroyed as the enhancement of the entropy around $T = \Delta$ squeezes the first Kondo screening sets at $\ln(2)$ as $T \to 0$. The LDOS, in turn, is progressively suppressed as Δ increases, confirming the destruction of both Kondo screening regimes. Also observe the progression of the U_{eff} as the Δ increases for $\Delta = 2 \times 10^{-6}$, $\Delta = 2 \times 10^{-5}$, $\Delta = 2 \times 10^{-4}$ and $\Delta = 2 \times 10^{-3}$ the second Hubbard peak occurs respectively in $\omega \approx 10^{-8}$, $\omega \approx 10^{-6}$, $\omega \approx 10^{-4}$ and $\omega \approx 10^{-3}$. This dependency can be understood by the previous section using PMS in SIAM, since it is shown in the Figure 7 we show that $\tilde{U}$ drops abruptly as the temperature decreases and we can associate this drop with the magnitude of $\Gamma(\Lambda)$ in equation (4.14). Notice now that below the gap $T < \Delta$, the hybridization function falls by several orders of magnitude, or in 'math' words $\Gamma(\Lambda > \Delta) \gg \Gamma(\Lambda < \Delta)$. So we can conclude that $\tilde{U}$ varies slowly within the gap and the smaller the Δ value, the lower values U_{eff} assumes.

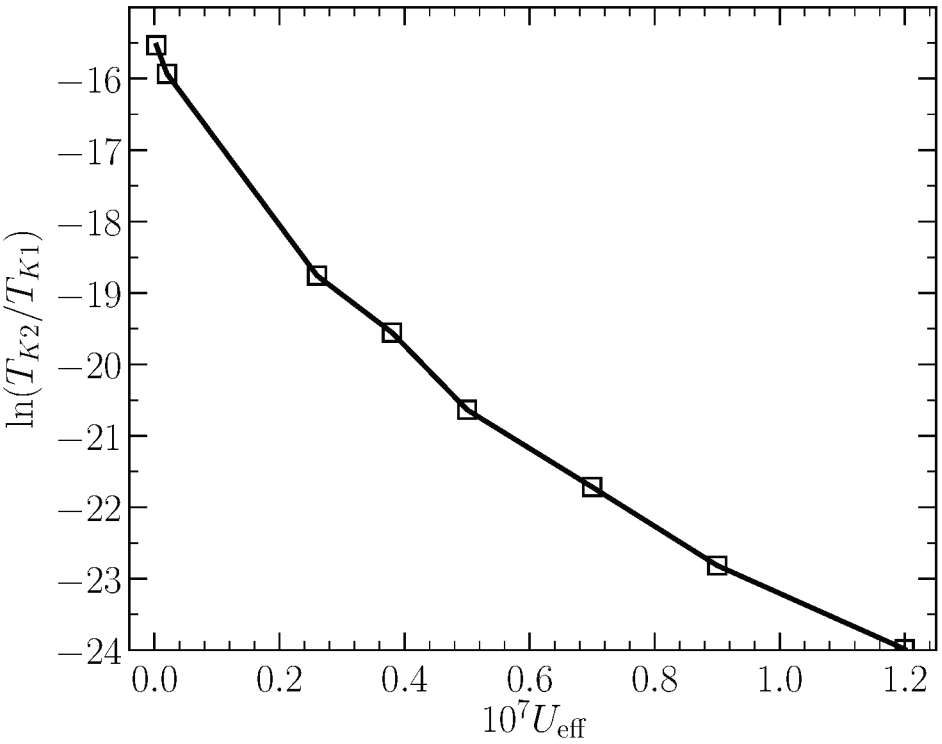

Figure 15 – $\ln(T_{K2}/T_{K1})$ vs U_{eff}. We expected a linear curve, like Figure 13 and then maybe we could infer an equation for T_{K2} like Haldane expression. However, the maximum that can be extracted from this result is $T_{K2} = B_0 g(U_{\text{eff}}) e^{-B_1 U_{\text{eff}}}$, where $g(x)$ is a some function.

As previous discussed we know that U_{eff} has a certain dependency with gap Δ, then, to change the U_{eff} value we change the Δ value, this dependency is shown in Figure 14(b) through the seconds Hubbard peaks. In Figure 15 we plot $\ln(T_{K2})$ x U_{eff}, But different from the result found in Figure 13, this curve is not linear. However, this unexpected result is not contradictory, in fact we can conclude that the behavior of T_{K2} with U_{eff} is in mostly

exponential. Then we can write $T_{K2} = B_0 g(U_{\text{eff}}) e^{-B_1 U_{\text{eff}}}$, where $g(x)$ is some function, which unfortunately we cannot find and the parameters B_0 and B_1 carry the intricate information from the renormalized effective Anderson model. Joining the information obtained through the graphs in the Figure 13 ($T_{K2} = A_0 e^{-A_1/\Gamma_M}$) and Figure 15 ($T_{K2} = B_0 g(U_{\text{eff}}) e^{-B_1 U_{\text{eff}}}$) also considering that U_{eff} and Γ_M are practically independent (see again the Figure 12). Then we can write T_{K2} with simultaneous dependence on U_{eff} and Γ_M as

$$T_{K2} = C_0 g(U_{\text{eff}}, \Gamma_M) e^{-C_1 \frac{U_{\text{eff}}}{\Gamma_M}}, \tag{5.3}$$

where $g(x, y)$ is some function, C_0 and C_1 are constants and all this terms carry the intricate information from the renormalized effective Anderson model. Unfortunately these results are only heuristic and we did not find anything like this equation through the PMS, in fact we do not even know if it is possible, since in energies scale below the T_{K1} perturbative methods don't work well.

The results shown so far are quite general and may be applicable to a variety of gapped systems to which a magnetic impurity can be coupled to. Examples encompass narrow-gap semiconductors [68], synthesized polymers [69], as well as modern gap-engineered materials [70]. In the following, we shall discuss how the reentrant SIAM behavior emerges in an AGNR in which a Rashba spin-orbit coupling (and thus a gap) is induced externally [71].

5.3 Thermodynamic properties for $\Gamma_M \sim \Gamma_S$

Here we discuss the case where the impurity is strongly coupled to the metallic-lead. To do this, the values of $\Delta = 10^{-5}$, $U = 0.5$, $\varepsilon_d = -0.25$ and $\Gamma_0 = 0.05$ are fixed. Remember in our definition of $\Gamma_0 = \Gamma_S + \Gamma_M$, then for fixed Γ_0, we have a dependency between Γ_S and Γ_M given by $\Gamma_S = \Gamma_0 - \Gamma_M$. This 'small' detail is important, since the $\Gamma_S \approx \Gamma_0$ approximation is no longer valid here. In addition, we will discuss in less detail about thermodynamic properties, since all this discussion has already been done in previous two sessions.

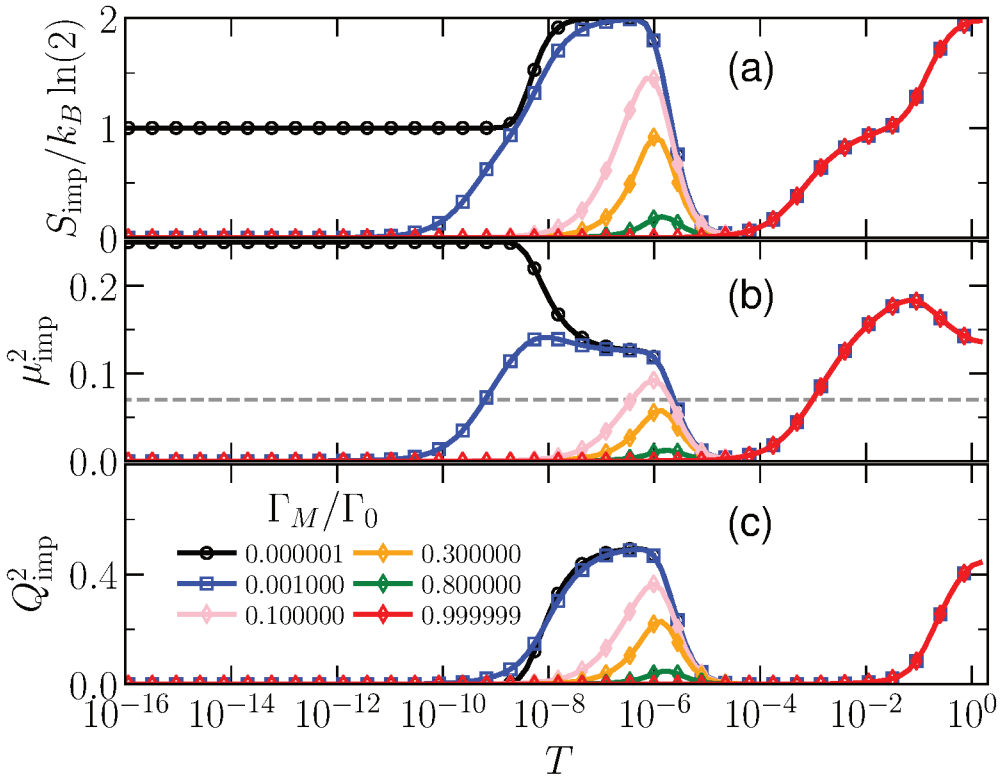

Figure 16 – Impurity contribution to (a) Entropy S_{imp}, (b) magnetic moment μ_{imp}, and (c) charge fluctuation ΔQ^2, as a function of temperature for $10^{-6}\Gamma_0 < \Gamma_M < \Gamma_0$. Note that the physics of the problem is the same as previews discussed in Figure 10. But here, we clearly observe the metallic behavior if $\Gamma_M \gg \Gamma_S$. See details in the text.

In Fig. 16 we show the impurity contribution to the entropy, S_{imp} [Fig. 16(a)], magnetic moment, μ^2_{imp} [Fig. 16(b)], as well as the charge fluctuations, Q^2_{imp} [Fig. 16(c)], as a function of temperature for $10^{-6}\Gamma_0 < \Gamma_M < \Gamma_0$. We first note that, for $\Gamma_M \approx \Gamma_0$ (in red) we observed the *traditional* metallic behavior (the thermodynamics proprieties do not change below T_K), since the impurity is practically uncoupled to the semiconductor-lead. Another case is for $\Gamma_M \approx 0$ (in black) where the impurity has coupled only to the semiconductor-lead (the same results obtained in Sec. 5.1). For $\Gamma_M = 0.001\Gamma_0$ (in blue), the impurity is weakly coupled to a metallic-lead and strongly coupled to a semiconductor-lead, condition in which we have the *reentrant* Kondo (as explained in details in Sec. 5.2).

However, for values in the same order of magnitude to Γ_M and Γ_S (in curves green, orange and pink), the contribution of impurity to thermodynamic properties has a competition between the singlet Kondo (due to the electrons in the metallic conduction band) and the valence-mixed state (due to the presence of the gap in the semiconductor band). To classify the impurity behavior as singlet Kondo or valence-mixed state, we use again the Wilson's criteria (represented by the horizontal gray line in [Fig. 16(b)]). Then, after this considerations, for $\Gamma_0 > \Gamma_M > 0.3\Gamma_0$ the impurity behavior are *majority* coupled to a metallic-lead, in which the semiconductor gap Δ was no significant importance to the system. And also for $0 < \Gamma_M < 0.1\Gamma_0$ the impurity behavior are *weakly* coupled to a metallic-lead.

5.4 NRG calculations for AGNR

In this section, we discuss a plausible experimental setup consisting of a magnetic impurity coupled to an AGNR, subjected to a tunable spin-orbit coupling, in which the phenomena presented in previews sections may be experimentally observed. It has been shown recently by Lenz et al. [71] that, under the influence of Rashba spin-orbit interaction (RSOI), due to an external electric field, or induced by a substrate, AGNRs exhibit a tunable band gap at the Fermi level [72]. In the following, we will consider a magnetic impurity coupled to such a gapped AGNR and weekly coupled to an STM tip (see Fig. 17). By employing a tight-binding model, combined with NRG calculations, we show that this setup is very convenient to investigate the *reentrant* Kondo effect. An AGNR may be metallic (when its width W, associated to N_A, is such that $N_A = 3M + 1$, where M is an integer), or semiconducting (for other values of N_A). The use of an *intrinsic* semiconducting AGNRs for the purpose of testing the reentrant Kondo effect would be problematic for two reasons: first, the typical gap values Δ that one obtains are in general *large*, and second, they are hard to tune. The proposal of using RSOI to produce a small and tunable gap Δ in a metallic AGNR, as illustrated in Fig. 17(b), sidesteps both problems at once.

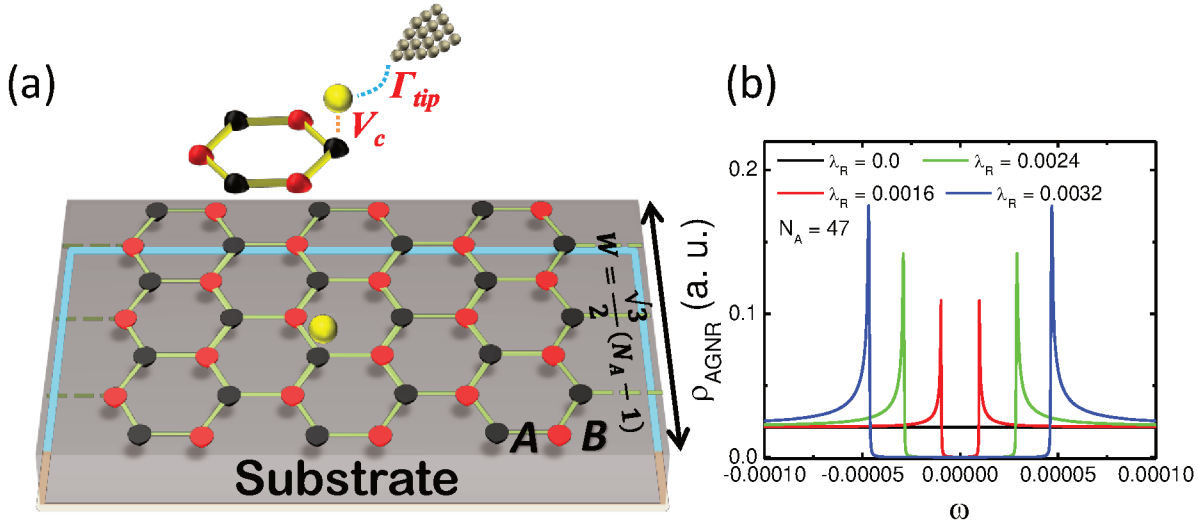

Figure 17 – (a) Schematic representation of an N_A-AGNR deposited on a substrate, with a magnetic impurity (yellow) deposited in a top-site configuration (right above a nanoribbon carbon atom (black), and strongly coupled to it, with hopping amplitude V_c). Right on top of the magnetic impurity adatom (as shown in the inset) is located a weakly coupled *metallic* STM tip, with a coupling strength Γ_{tip}. (b) DOS for a 47-AGNR close to the Fermi level, without the impurity, as a function of energy ω, for different RSOI strengths λ_R. W is the width of the AGNR (assuming a nearest-neighbor distance $a_{c-c} = 1$), which depends on the number of dimmers, N_A, across the nanoribbon. Note that, as $N_A = 47 = 3 \times 16 - 1$, the $\lambda_R = 0.0$ DOS (black curve) is metallic, while a finite λ_R opens a gap in the spectra.

For concreteness, we consider a metallic AGNR, of width $W = \sqrt{3}\,(N_A - 1)\,/2$, where N_A is the number of dimmers along the transverse direction [see Fig. 17(a) for details]. Figure 17(b) shows the density of states $\rho_{\mathrm{AGNR}}(\omega)$ close to the Fermi level, for a pristine nanoribbon, i.e., without any impurity coupled to its surface, for different values of RSOI. We clearly see that in the absence of RSOI ($\lambda_R = 0$) our AGNR exhibits a gapless DOS as shown by the black line in Fig. 17(b). However, a finite λ_R induces a gap Δ around the Fermi level as shown by the red ($\lambda_R = 1.6 \times 10^{-3}$), green ($\lambda_R = 2.4 \times 10^{-3}$), and blue ($\lambda_R = 3.2 \times 10^{-3}$) curves in Fig. 19(b), for progressively larger values of λ_R. Thus, the AGNR with finite RSOI simulates the semiconducting band coupled to the impurity, while the STM tip plays the role of the metallic band defined in Chapter 4, introducing a small but finite broadening of the impurity level, Γ_{M}, inside the gap.

In what follows, we have set $\Gamma_{\mathrm{M}} = 1.0 \times 10^{-6}$ (thus, fixing V_{tip}) and the AGNR-impurity coupling $V_C = 0.258$, considering $N_A = 47$. Therefore, we considered the impurity position fixed at a given top-site location [73] for all the following calculations. The resulting hybridization function, for various values of λ_R, is shown in Fig. 18. To make the region near the Fermi level (located slightly to the left of the left axis) more visible, we plot the energy axis in log-scale, restricted to $\omega > 0$ [by virtue of particle-hole symmetry, we have that $\Gamma_0(-\omega) = \Gamma_0(\omega)$]. As expected, for $\lambda_R = 0.0$ the AGNR is metallic, therefore

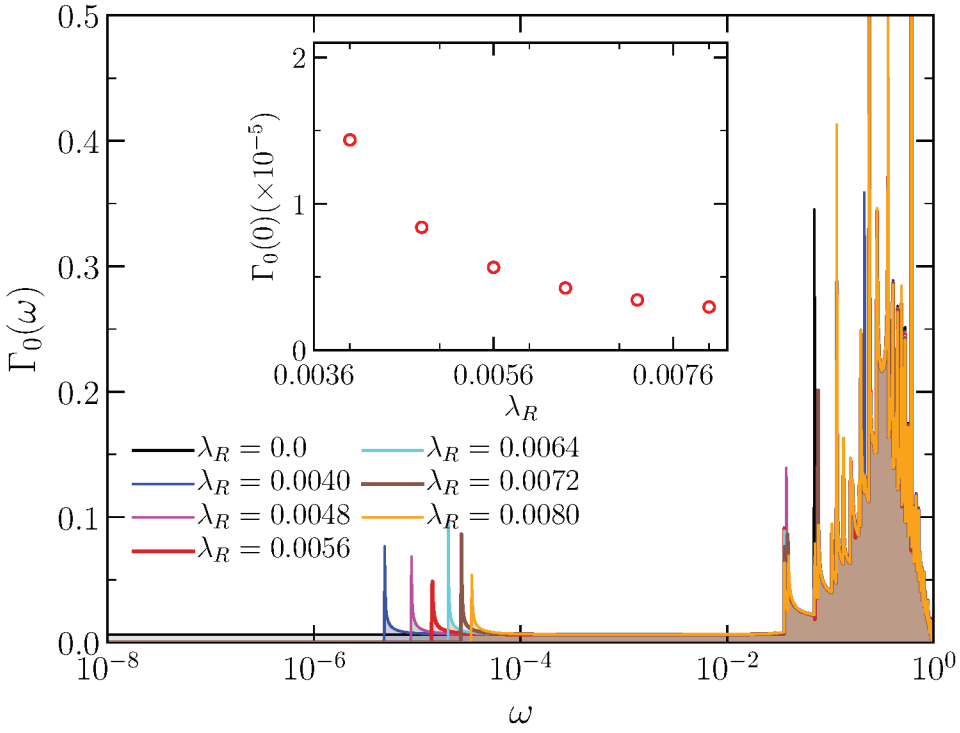

Figure 18 – Hybridization function $\Gamma_0(\omega)$ for vanishing λ_R (black curve) and in the interval $0.004 \leq \lambda_R \leq 0.008$. The range of values of λ_R was chosen in order to produce Δ values monotonically increasing with λ_R. The inset shows the value of $\Gamma_0(0)$ as a function of λ_R. Parameter values are $V_C = 0.258$ and $\Gamma_M = 10^{-6}$.

$\Gamma_0(\omega)$ has a constant value (≈ 0.01) around the Fermi level. In this case, our system behaves quite similarly to a QI coupled to a metallic DOS with a flat band. However, for finite λ_R we clearly see the formation of a small gap Δ, which increases with λ_R. In the inset of Fig. 18 we show how $\Gamma_0(0)$ evolves with λ_R. We note that $\Gamma_0(0)$ has a small residual and finite value inside the RSOI induced gap, originated from the *localized* impurity state contribution, which decreases as λ_R (or Δ) increases, eventually saturating at $\Gamma_0(0) \approx \Gamma_{\text{tip}} = 10^{-6}$ (or Γ_{M}).

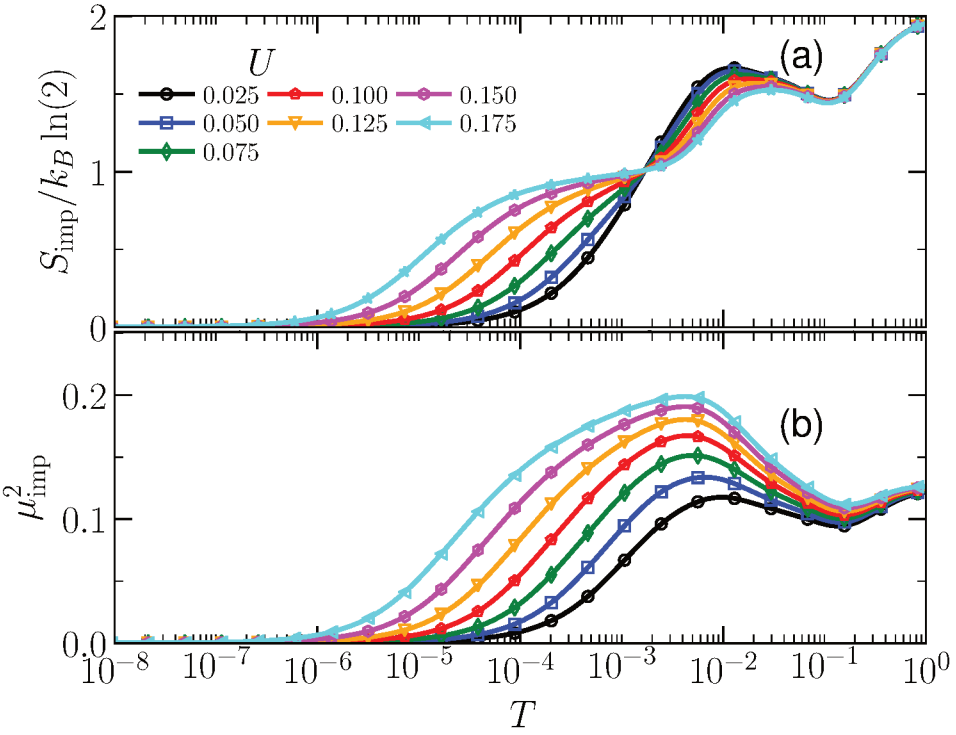

Figure 19 – Entropy (a) and magnetic moment (b) for a metallic 47-AGNR ($\lambda_R = 0.0$) as a function of temperature, for different values of U. Remaining parameter values are the same as in Fig. 18.

Before studying how the induced gap affects the Kondo screening in the system, let us first analyze the Kondo effect in the absence of RSOI, and then see how it is modified by a finite RSOI. In Fig. 19, we show, in panel (a), the impurity entropy contribution, S_{imp}, and in panel (b) the magnetic moment, μ^2_{imp}, for $\lambda_R = 0.0$ and $0.025 \leq U \leq 0.175$. As expected, the characteristic behavior of the SIAM is observed as the temperature is lowered, namely, the crossovers from FO to the unstable LM, and then from the LM to the SC. For small values of U, such as $U = 0.025$ (black curve), the LM fixed point is not visible, as in this case the Kondo temperature becomes comparable to Γ, U, and the system is close to an intermediate valence situation. The intriguing small dip in the impurity magnetic moment, as well as in the entropy, for temperatures in the range $10^0 - 10^{-2}$, points to the presence of van-Hove singularities [74], coming from the quasi-1D band structure of the AGNR, which has a small variation for the different U values considered.

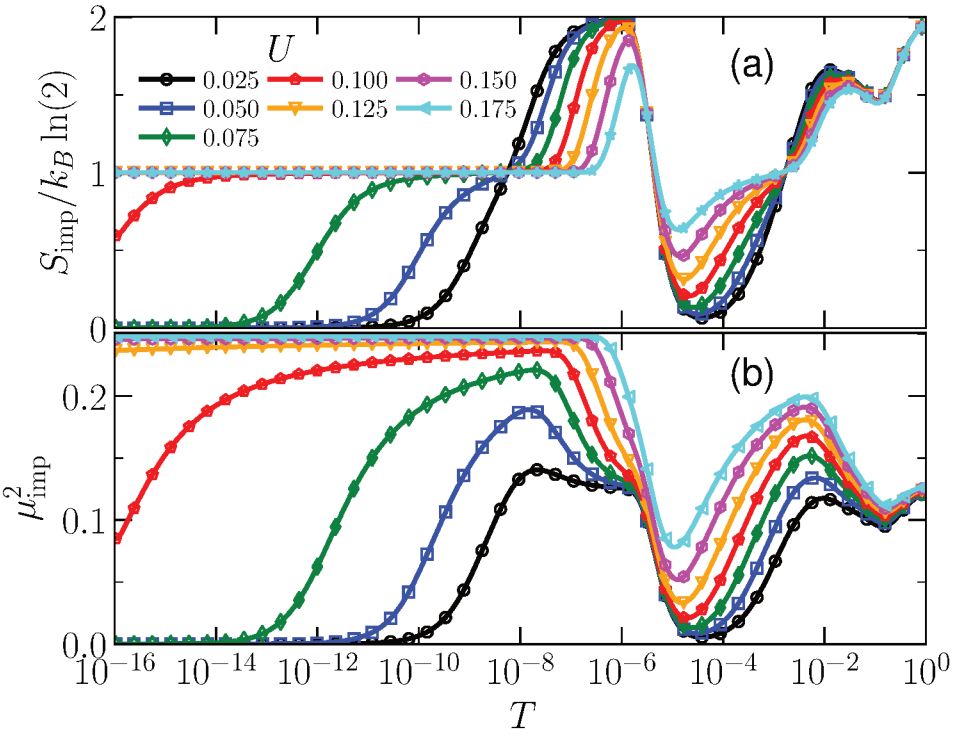

Figure 20 – Impurity entropy (a) and magnetic moment (b) for a 47-AGNR as a function of temperature, for fixed RSOI induced gap ($\Delta = 0.9 \times 10^{-5}$) and different values of U.

To see how the gap-opening introduces the reentrant SIAM behavior, discussed in Sec. 5.2, in Fig. 20 we repeat the calculations shown in Fig. 19, with the same set of parameters, except that λ_R is now finite, producing a gap $\Delta = 0.9 \times 10^{-5}$. For values of $U = 0.025$, up to $U = 0.075$, we clearly see, both from the entropy [Fig. 21(a)] and from the magnetic moment [Fig. 21(b)], the emergence of the reentrant SIAM behavior for temperatures below $\Delta \approx 10^{-5}$ (compare with the results in Fig. 19 for the same temperature range). As U increases, the Kondo temperature T_{K1} of the first Kondo screening decreases, so that the unstable LM fixed point becomes more pronounced (i.e., extends over a larger interval of temperature). As a consequence, the observed decrease of T_{K1}, as U increases, squeezes the first SC fixed point within a temperature range $\Delta \lesssim T \lesssim T_{K1}$, and, eventually, the first Kondo screening ceases to occur when T_{K1} becomes comparable to Δ. This is manifested in the progressive enhancement of $S_{\rm imp}$ and $\mu^2_{\rm imp}$ in this temperature region (because the first LM fixed point extends further down in temperature). It is interesting to observe that the reentrant Kondo temperature T_{K2} decreases much more rapidly than T_{K1} with increasing U, as observed in the fast increase of plateau extension of the reentrant LM fixed point. The decrease of T_{K1} with increasing U can be understood in terms of the Haldane expression for the Kondo temperature in the conventional SIAM [59]. From our calculations we find that the effective Coulomb repulsion $U_{\rm eff}$ increases by increasing U. Thus, even though the Haldane expression cannot be readily applied to obtain T_{K2}, it

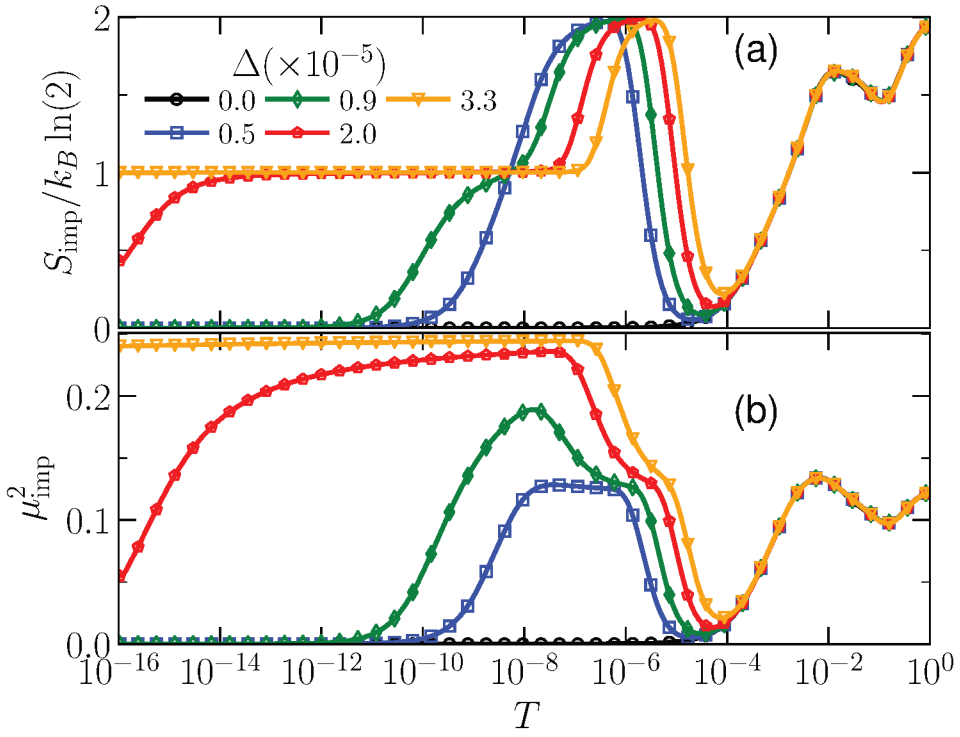

Figure 21 – Impurity entropy (a) and magnetic moment (b) for a 47-AGNR as a function of temperature, for different values of RSOI induced gap ($\Delta \approx \lambda_R$). The parameter values for both panels are $\Gamma_M = 1.0 \times 10^{-6}$ and $U = 0.05$.

provide us with a good insight on why T_{K2} decreases rapidly by increasing U.

Finally, we study how the reentrant SIAM behavior is modified by changing the AGNR gap. Fig. 21(a) and 21(b) show, respectively, $S_{\rm imp}$ and $\mu^2_{\rm imp}$ as a function of T, for a fixed value $U = 0.05$ and $0 \leq \Delta \leq 3.3 \times 10^{-5}$. After interpreting the results in Fig. 20, as done above, where we fixed Δ and increased U, the results in Fig. 21 can be understood quite straightforwardly. Indeed, by increasing Δ, the extension of the first LM fixed point is squeezed from below, as T_{K1} is now fixed (notice the collapse of all curves, in both panels, for $T \gtrsim 10^{-4}$), and the extent of the first SC fixed point is determined by Δ. In addition, the extension of the reentrant FO fixed point plateau decreases for increasing Δ, indicating a decrease in the charge fluctuations in the reentrant SIAM for increasing Δ. This suggests that the effective Coulomb repulsion $U_{\rm eff}$ associated to the reentrant SIAM increases with Δ, resulting in smaller T_{K2} values, which is clearly seen by the reentrant Kondo screening taking place at lower temperatures for larger Δ. Finally, for $\Delta \gg T_{K1}$ (not shown), no Kondo screening takes place as Δ exceeds T_K (which is analogous to say that $\Gamma_C > \Gamma_0$) destroying the first Kondo stage, as discussed in Chapter 4.

6 Conclusion

In this work, we studied the behavior of a magnetic impurity coupled to several conduction band structures (metallic band, pseudo-gap systems and semiconductors with finite gap). Besides that the magnetic impurity can be coupled to more than one lead. However, the main focus is to explain the behavior of a magnetic impurity coupled with two leads, one metallic and one semiconductor. For this reasons, we used Anderson Model for one or more conduction bands coupled to the impurity. Then, we started by deriving the Kondo model from the Anderson Model using the projection operators and restricting the Hamiltonian in the conditions necessary for the Kondo effect occur, thus, we show that Kondo Model is a particular case of Anderson Model in Local Moment regime. Using the scattering Matrix (T-Matrix) and following Anderson's ideas we derive the scaling equations for the Kondo Hamiltonian known as Poor man's scaling in Kondo Model. The Poor man's scaling is a perturbative method and after the long calculations to find the β-equation is easy to get some information from the system. Only with conduction band information and impurity energy levels we can find J_C and T_K. The results found by Poor Man's scaling, although limited to temperature scales above T_K and extract only some information, are satisfactory if compared to the NRG. We use this equation to estimate the characteristic Kondo temperature T_K for each of the described conduction bands. We also find the conditions under which the Kondo effect can occur, known as critical coupling J_C. However, for temperatures below the T_K we need a non-degenerate technique to solve this problems, the ideal tool to do this is the NRG. For the metallic conduction band and also for the pseudo-gap system, they are extensively explored in the literature. However, for the semiconductor it has only few works.

In our calculations for the semiconductor band, in the first NRGs results we had evidence to the reentrant SIAM for temperatures scale below the gap. Then, to understand this behavior we use the poor man's scaling in the Anderson Model. To do this it was necessary to use second order non-degenerate perturbation theory in SIAM, then we find the scaling equations for this parameters $\tilde{U}$, $\tilde{\varepsilon}_d$ and $\tilde{\Gamma}$. Next we use this scaling equations to understand the behavior of the magnetic impurity coupled structured conduction band and we came to the conclusion that below the gap, there could really be a 'second' SIAM with renormalized parameters, but the poor man's scaling not enough. We compared the result obtained for Γ_C using NRG and PMS, the results were close, with similar behavior, but they are not identical, in fact this was not expected. We also came to the conclusion that in this system there may be a transient Kondo (unstable SC fixed point), but the fundamental state must be a doublet.

Later, we modified the system to study using only NRG an impurity coupled with a semiconductor lead and weakly coupled with a metallic lead. In this system it is clear the repetition of all fixed points, including a second regime of strong coupling fixed point (a second Kondo effect occur below the gap). Using LDOS in NRG we were able to estimate U_{eff} by locating the second Hubbard peak, also the second Kondo peak. In addition, we note that U_{eff} is independent of Γ_{M}, but is extremely dependent on Γ_0 and Δ. We observed that in this system, for finite Γ_{M} and forming the first SC fixed point (unstable SC fixed point), then the ground state is the singlet Kondo (stable SC fixed point). We also note the exponential behavior of T_{K2} with Γ_{M}, similar to Haldane's expression. Besides that the behavior of the T_{K2} with U_{eff} are also majority exponential, but carries an unknown term that depends of the U_{eff}. Putting the previous information together, we found an approximate heuristic expression for T_{K2}, but unfortunately we can not validate this through analytical calculations yet.

The system consisting by the magnetic impurity coupled to an AGNR, subjected to a tunable spin-orbit coupling, in which the *reentrant* SIAM may be experimentally observed. For typical values of this system, we can find $T_{K1} = 55K$ and $T_{K2} = 10mK$. In addition, we can find several other systems with a small gap, where this study can be applied. Future perspective: Our finding may be useful to understand the Kondo problem in gapped materials such as Dirac insulators [75, 76], in which the conduction band exhibit a small gap.

Bibliography

[1] Lei Liang. *Field effect controlled magnetism and magnetotransport in low dimensions*. PhD thesis, University of Groningen, 2017. Available at https://research.rug.nl/en/publications/field-effect-controlled-magnetism-and-magnetotransport-in-low-dim. 8, 17

[2] G. R. SOUSA. Impurezas quânticas em sistemas com interação spin-órbita. dissertação – infis, universidade federal de uberlândia. uberlândia. 2016. Available at https://repositorio.ufu.br/handle/123456789/18117. 9, 28

[3] P W Anderson. More Is Different. *Science*, 177:393, 1972. https://doi.org/10.1126/science.177.4047.393. 13

[4] Jun Kondo. Resistance Minimum in Dilute Magnetic Alloys. *Prog. Theor. Phys.*, 32(1):37, 1964. https://doi.org/10.1143/PTP.32.37. 13, 18, 20

[5] A. C. Hewson. *The Kondo problem to heavy fermions*. Cambridge University Press, 1993. Available at https://doi.org/10.1017/CBO9780511470752. 13, 14, 20, 38, 45, 48, 52

[6] Kenneth G. Wilson. The renormalization group: Critical phenomena and the kondo problem. *Rev. Mod. Phys.*, 47:773–840, Oct 1975. https://link.aps.org/doi/10.1103/RevModPhys.47.773. 13, 14, 36

[7] W. J. de Haas, J. H. de Boer, and G. J. van den Berg. *Physica*, 1, 1934. https://doi.org/10.1016/S0031-8914(34)80310-2. 13

[8] G. J. van den Berg. *Progress in Low Temperature Physics*, IV:194, 1964. https://doi.org/10.1016/S0079-6417(08)60152-3. 13

[9] Sara M. Cronenwett, Tjerk H. Oosterkamp, and Leo P. Kouwenhoven. A tunable kondo effect in quantum dots. *Science*, 281(5376):540–544, 1998. https://doi.org/10.1126/science.281.5376.540. 13

[10] J. Martinek, Y. Utsumi, H. Imamura, J. Barnaś, S. Maekawa, J. König, and G. Schön. Kondo effect in quantum dots coupled to ferromagnetic leads. *Phys. Rev. Lett.*, 91:127203, Sep 2003. https://link.aps.org/doi/10.1103/PhysRevLett.91.127203. 13

[11] Michael Pustilnik and Leonid Glazman. Kondo effect in quantum dots. *Journal of Physics: Condensed Matter*, 16(16):R513–R537, apr 2004. https://doi.org/10.1088/0953-8984/16/16/R01. 13

[12] D Boese and R Fazio. Thermoelectric effects in kondo-correlated quantum dots. *Europhysics Letters (EPL)*, 56(4):576–582, nov 2001. https://doi.org/10.1209/epl/i2001-00559-8. 13

[13] Leo Kouwenhoven and Leonid Glazman. Revival of the kondo effect. *Physics World*, 14(1):33–38, jan 2001. https://doi.org/10.1088/2058-7058/14/1/28. 13

[14] Kicheon Kang, Sam Young Cho, Ju-Jin Kim, and Sung-Chul Shin. Anti-kondo resonance in transport through a quantum wire with a side-coupled quantum dot. *Phys. Rev. B*, 63:113304, Feb 2001. https://link.aps.org/doi/10.1103/PhysRevB.63.113304. 13

[15] P. S. Cornaglia, H. Ness, and D. R. Grempel. Many-body effects on the transport properties of single-molecule devices. *Phys. Rev. Lett.*, 93:147201, Sep 2004. https://link.aps.org/doi/10.1103/PhysRevLett.93.147201. 13

[16] V. Ravi Chandra, Sumathi Rao, and Diptiman Sen. Renormalization group study of the kondo problem at a junction of several luttinger wires. *Phys. Rev. B*, 75:045435, Jan 2007. https://link.aps.org/doi/10.1103/PhysRevB.75.045435. 13

[17] Yasuhiro Utsumi, Jan Martinek, Gerd Schön, Hiroshi Imamura, and Sadamichi Maekawa. Nonequilibrium kondo effect in a quantum dot coupled to ferromagnetic leads. *Phys. Rev. B*, 71:245116, Jun 2005. https://link.aps.org/doi/10.1103/PhysRevB.71.245116. 13

[18] D Goldhaber-Gordon, H Shtrikman, D Mahalu, D Abusch-Magder, U Meirav, and MA Kastner. Kondo effect in a single-electron transistor. *Nature*, 391:156, 1998. https://doi.org/10.1038/34373. 13

[19] A. A. Houck, J. Labaziewicz, E. K. Chan, J. A. Folk, and I. L. Chuang. Kondo effect in electromigrated gold break junctions. *Nano Letters*, 5(9):1685–1688, 2005. Disponívelem:https://doi.org/10.1021/nl050799i. 13

[20] A. K. Mitchell, D. Schuricht, M. Vojta, , and L. Fritz. Kondo effect on the surface of three-dimensional topological insulators: Signatures in scanning tunneling spectroscopy. *Phys. Rev. B*, 87:075430, 2013. https://doi.org/10.1103/PhysRevB.87.075430. 13

[21] Minh-Tien Tran and Ki-Seok Kim. Probing surface states of topological insulators: Kondo effect and friedel oscillations in a magnetic field. *Phys. Rev. B*, 82:155142, Oct 2010. https://link.aps.org/doi/10.1103/PhysRevB.82.155142. 13

[22] L. Isaev, G. Ortiz, and I. Vekhter. Tunable unconventional kondo effect on topological insulator surfaces. *Phys. Rev. B*, 92:205423, Nov 2015. https://link.aps.org/doi/10.1103/PhysRevB.92.205423. 13

[23] Bushra Irfan and Ratnamala Chatterjee. Magneto-transport and kondo effect in cobalt doped bi2se3 topological insulators. *Applied Physics Letters*, 107(17):173108, 2015. https://doi.org/10.1063/1.4934569. 13

[24] B. Béri and N. R. Cooper. Topological kondo effect with majorana fermions. *Phys. Rev. Lett.*, 109:156803, Oct 2012. https://link.aps.org/doi/10.1103/PhysRevLett.109.156803. 13

[25] Xianhao Xin and Di Zhou. Kondo effect in a topological insulator quantum dot. *Phys. Rev. B*, 91:165120, Apr 2015. https://link.aps.org/doi/10.1103/PhysRevB.91.165120. 13

[26] H. R. Krishna-murthy, J. W. Wilkins, and K. G. Wilson. Renormalization-group approach to the anderson model of dilute magnetic alloys. i. static properties for the symmetric case. *Phys. Rev. B*, 21:1003, 1980. https://doi.org/10.1103/PhysRevB.21.1003. 13, 14

[27] C. Lacroix. Density of states for the asymmetric anderson model. *Journal of Applied Physics*, 53(3):2131–2133, 1982. https://doi.org/10.1063/1.330756. 14

[28] R. Frésard and T. Kopp. Exact results with the kotliar-ruckenstein slave-boson representation. *Annalen der Physik*, 524(3-4):175–181, 2012. http://dx.doi.org/10.1002/andp.201100197. 14

[29] D. L. Cox and A. Zawadowski. Exotic kondo effects in metals: Magnetic ions in a crystalline electric field and tunnelling centres. *Advances in Physics*, 47(5):599–942, 1998. https://doi.org/10.1080/000187398243500. 14

[30] N. Andrei, K. Furuya, and J. H. Lowenstein. Solution of the kondo problem. *Rev. Mod. Phys.*, 55:331–402, Apr 1983. https://link.aps.org/doi/10.1103/RevModPhys.55.331. 14

[31] P. W. Anderson. *Phys. Rev.*, 109:1492, 1958. https://doi.org/10.1103/PhysRev.109.1492. 14

[32] M. Cheng, T. Chowdhury, A. Mohammed, and K. Ingersent. Phase boundaries of power-law Anderson and Kondo models: A poor man's scaling study. *Phys. Rev. B*, 96:045103, 2017. https://doi.org/10.1103/PhysRevB.96.045103. 14, 30, 31, 34, 40, 51

[33] Ralf Bulla, Theo A. Costi, and Thomas Pruschke. Numerical renormalization group method for quantum impurity systems. *Rev. Mod. Phys.*, 80:395, 2008. https://doi.org/10.1103/RevModPhys.80.395. 14

[34] Kan Chen and C Jayaprakash. The kondo effect in pseudo-gap fermi systems: a renormalization group study. *Journal of Physics: Condensed Matter*, 7(37):L491–L498, sep 1995. 14

[35] Luis G. G. V. Dias da Silva, Nancy Sandler, Pascal Simon, Kevin Ingersent, and Sergio E. Ulloa. Tunable pseudogap kondo effect and quantum phase transitions in aharonov-bohm interferometers. *Phys. Rev. Lett.*, 102:166806, Apr 2009. https://link.aps.org/doi/10.1103/PhysRevLett.102.166806. 14

[36] Matthias Vojta and Lars Fritz. Upper critical dimension in a quantum impurity model: Critical theory of the asymmetric pseudogap kondo problem. *Phys. Rev. B*, 70:094502, Sep 2004. https://link.aps.org/doi/10.1103/PhysRevB.70.094502. 14

[37] C. Gonzalez Buxton and K. Ingersent. *Phys. Rev. B*, 57:14254, 1998. https://doi.org/10.1103/PhysRevB.57.14254. 14

[38] L. Cruz, P. Phillips, and A. H. Castro Neto. Kondo resonance and logt conductivity in highly conducting trans-polyacetylene. *Europhys. Lett.*, 29:389–394, 1995. https://doi.org/10.1209/0295-5075/29/5/007. 14, 37

[39] Jimin Kim et. all. Observation of tunable band gap and anisotropic Dirac semimetal state in black phosphorus. *Science*, 349:723–726, 2015. https://doi.org/10.1126/science.aaa6486. 14

[40] Katsunori Wakabayashi, Yositake Takane, Masayuki Yamamoto, and Manfred Sigrist. Electronic transport properties of graphene nanoribbons. *New J. Phys.*, 11(9):095016, 2009. https://doi.org/10.1088/1367-2630/11/9/095016. 15

[41] C. A. Büsser, G. B. Martins, and A. E. Feiguin. Lanczos transformation for quantum impurity problems in d-dimensional lattices: Application to graphene nanoribbons. *Phys. Rev. B*, 88:245113, 2013. https://doi.org/10.1103/PhysRevB.88.245113. 15

[42] Damian Krychowski, Jakub Kaczkowski, and Stanislaw Lipinski. Kondo effect of a cobalt adatom on a zigzag graphene nanoribbon. *Phys. Rev. B*, 89:035424, Jan 2014. https://link.aps.org/doi/10.1103/PhysRevB.89.035424. 15

[43] Yang Li, Anh T. Ngo, Andrew DiLullo, Kyaw Zin Latt, Heath Kersell, Brandon Fisher, Peter Zapol, and Saw-Wai Ulloa, Sergio E.and Hla. Anomalous kondo resonance

mediated by semiconducting graphene nanoribbons in a molecular heterostructure. *Nat. Commun.*, 8:946, 2017. https://doi.org/10.1038/s41467-017-00881-1. 15

[44] G. S. Diniz, G. I. Luiz, A. Latgé, and E. Vernek. From kondo to local singlet state in graphene nanoribbons with magnetic impurities. *Phys. Rev. B*, 97:115444, Mar 2018. https://link.aps.org/doi/10.1103/PhysRevB.97.115444. 15

[45] Katsuhiko Takegahara, Yukihiro Shimizu, and Osamu Sakai. Quantum monte carlo and numerical renormalization group studies of magnetic impurities in nonmetallic systems. *J. Phys. Soc. Jpn.*, 61:3443, 1992. https://doi.org/10.1143/JPSJ.61.3443. 15

[46] Katsuhiko Takegahara, Yukihiro Shimizu, Naoya Goto, and Osamu Sakai. Magnetic impurity in nonmetallic systems. *Physica B*, 186:381, 1993. https://doi.org/10.1143/JPSJ.61.3443. 15

[47] Tetsuro Saso. 1/n and quantum monte carlo studies of a magnetic impurity in an insulator with a small gap. *J. Phys. Soc. Jpn.*, 61(10):3439, 1992. https://doi.org/10.1143/JPSJ.61.3439. 15

[48] Jun Ogura and Tetsuro Saso. Magnetic impurity in insulators with small energy gap. *J. Phys. Soc. Jpn.*, 62:4364, 1993. https://doi.org/10.1143/JPSJ.62.4364. 15

[49] L. Cruz, P. Phillips, and A. H. Castro Neto. Kondo resonance and logt conductivity in highly conducting trans-polyacetylene. *EPL*, 29:389, 1995. https://doi.org/10.1209/0295-5075/29/5/007. 15

[50] Clare C. Yu and M. Guerrero. Anderson impurity in a semiconductor. *Phys. Rev. B*, 54:8556, 1996. https://doi.org/10.1103/PhysRevB.54.8556. 15

[51] Kan Chen and C. Jayaprakash. Kondo effect in Fermi systems with a gap: A renormalization-group study. *Phys. Rev. B*, 57:5225, 1998. https://doi.org/10.1103/PhysRevB.57.5225. 15

[52] C. P. Moca and A. Roman. Quantum phase transition in a gapped anderson model: A numerical renormalization group study. *Phys. Rev. B*, 81:235106, 2010. https://doi.org/10.1088/0953-8984/7/37/003. 15

[53] Martin R. Galpin and David E. Logan. Anderson impurity model in a semiconductor. *Phys. Rev. B*, 77:195108, 2008. https://doi.org/10.1103/PhysRevB.77.195108. 15, 46

[54] M. R. Galpin and D. E. Logan. A local moment approach to the gapped anderson model. *Eur. Phys. J. B*, 62:129, 2008. https://doi.org/10.1140/epjb/e2008-00138-5. 15, 46

[55] C. A. Kukkonen. T^2 electrical resistivity due to electron-phonon scattering on a small cylindrical Fermi surface: Apphcation to bismuth. *Physical Review B*, 18, 1978. https://doi.org/10.1103/PhysRevB.18.1849. 18

[56] J. Bardeen, L. N. Cooper, and J. R. Schrieffer. Theory of superconductivity. *Phys. Rev.*, 108:1175–1204, Dec 1957. https://link.aps.org/doi/10.1103/PhysRev.108.1175. 18

[57] E. Pavarini, E. Koch, and P. Coleman. Many-body physics: From kondo to hubbard modeling and simulation. 5, 2015. Available at http://juser.fz-juelich.de/record/205123. Acessed in 01/23/2020. 26

[58] P W Anderson. A poor man's derivation of scaling laws for the kondo problem. *J. Phys. C: Sol. St. Phys.*, 3:2436, 1970. https://doi.org/10.1088/0022-3719/3/12/008. 27, 38

[59] F. D. M. Haldane. Scaling theory of the asymmetric anderson model. *Phys. Rev. Lett.*, 40:416, 1978. https://doi.org/10.1103/PhysRevLett.40.416. 29, 51, 60

[60] Adrian Roman and Computational Physics Blog. The Numerical Renormalization Group. Available at https://compphys.go.ro/the-numerical-renormalization-group/. Accessed in: 01/23/2020. 36

[61] E. Pavarini, E. Koch, F. Anders, and M. Jarrell. The numerical renormalization group. *Correlated Electrons: From Models to Materials Modeling and Simulation*, 2:12.2, 2012. Available at https://www.cond-mat.de/events/correl12/manuscripts/correl12.pdf. 36

[62] Rok Zitko and Thomas Pruschke. Energy resolution and discretization artefacts in the numericalrenormalization group. *Phys. Rev. B*, 79:085106, 2009. https://link.aps.org/doi/10.1103/PhysRevB.79.085106. 36, 42

[63] Rok Zitko. Numerical renormalization group calculations of ground-state energy: Application to correlation effects in the adsorption of magnetic impurities on metal surfaces. *Phys. Rev. B*, 79:233105, 2009. https://doi.org/10.1103/PhysRevB.79.233105. 36, 42

[64] Mengxing Cheng and Kevin Ingersent. Quantum phase transitions in a pseudogap Anderson-Holstein model. *Phys. Rev. B*, 87:075145, 2013. https://doi.org/10.1103/PhysRevB.87.075145. 40, 51

[65] D N Zubarev. Double-time green functions in statistical physics. *Phys.-Uspekhi*, 3(3):320–345, mar 1960. https://doi.org/10.1070/PU1960v003n03ABEH003275. 50

[66] Frithjof B. Anders and Avraham Schiller. Spin precession and real-time dynamics in the kondo model: Time-dependent numerical renormalization-group study. *Phys. Rev. B*, 74:245113, Dec 2006. https://link.aps.org/doi/10.1103/PhysRevB.74.245113. 50

[67] J H Jefferson. A renormalisation group approach to the mixed valence problem. *J. Phys. C: Sol. St. Phys.*, 10(18):3589–3599, sep 1977. https://doi.org/10.1088/0022-3719/10/18/023. 51

[68] S. Massidda, A. Continenza, A. J. Freeman, T. M. de Pascale, F. Meloni, and M. Serra. Structural and electronic properties of narrow-band-gap semiconductors: Inp, inas, and insb. *Phys. Rev. B*, 41:12079, 1990. https://doi.org/10.1103/PhysRevB.41.12079. 54

[69] A. J. Heeger, S. Kivelson, J. R. Schrieffer, and W. P. Su. Solitons in conducting polymers. *Rev. Mod. Phys.*, 60:781, 1988. https://doi.org/10.1103/RevModPhys.60.781. 54

[70] Sven Borghardt, Jhih Sian Tu, Florian Winkler, Jurgen Schubert, Willi Zander, Kristjan Leosson, and Beata E. Kardyna. Engineering of optical and electronic band gaps in transition metal dichalcogenide monolayers through external dielectric screening. *Phys. Rev. Materials*, 1:1, 2017. https://doi.org/10.1103/PhysRevMaterials.1.054001. 54

[71] Lucia Lenz, Daniel F. Urban, and Dario Bercioux. Rashba spin-orbit interaction in graphene armchair nanoribbons. *Eur. Phys. J. B*, 86:502, 2013. https://doi.org/10.1140/epjb/e2013-40760-4. 54, 57

[72] Note: Depending on the number of dimmers along the transverse direction, the AGNR can be metallic or an *intrinsic* semiconductor. In what follows, we will explore the extrinsic tunable induced gap in metallic AGNR by means of an external agent. 57

[73] Note: Co adatoms, deposited on monolayer graphene (deposited, in turn, over a SiC (0001) substrate), have shown to be most favorable in a top-site configuration (see Fig. 17), as experimentally reported by Eelbo *et al.*, Phys. Rev. Lett. 110, 136804 (2013). 58

[74] Note: The Van-Hove singularities are fixed for a given λ_R, however, as λ_R is varied (for the range of λ_R considered), the first peak is strongly modified, as one can note in Fig.18. 59

[75] D. Hsieh, D. Qian, L. Wray, Y. Xia, Y. S. Hor, R. J. Cava, and M. Z. Hasan. A topological dirac insulator in a quantum spin hall phase. *Nature*, 452(7190):970–974, 2008. https://doi.org/10.1038/nature06843. 63

[76] S. R. Yang, Y. T. Fanchiang, C. C. Chen, C. C. Tseng, Y. C. Liu, M. X. Guo, M. Hong, S. F. Lee, and J. Kwo. Evidence for exchange Dirac gap in magnetotransport of topological insulator-magnetic insulator heterostructures. *PhysRevB.*, 100:045138, 2019. https://doi.org/10.1103/PhysRevB.100.045138. 63